Magmatism, migrating topography, and the onset of Basin and Range faulting

Jens-Erik Lund Snee[1] and Elizabeth L. Miller[2]

[1]Department of Geophysics, Stanford University, 397 Panama Mall, Mitchell Bld. 3rd Floor, Stanford, CA 94305

[2]Department of Geological Sciences, Stanford University, 450 Serra Mall Bld. 320, Room 118, Stanford, CA 94305

KEY POINTS:

- Before the middle Eocene, the Sevier hinterland lay east of the axis of the Cretaceous Sierran arc and was underlain by 50 km thick crust.
- Thermally driven uplift and southward migrating magmatism shifted the paleodivide to central Nevada in the Eocene.
- Changing boundary conditions caused Miocene extension of thermally weakened crust, rather than collapse of a high Cretaceous Nevadaplano.

ABSTRACT

According to a widely applied model, Cenozoic extension in the Great Basin was driven by collapse of a high plateau supported by crustal thicknesses at least double the present ~30 km. Despite widespread use, this model has been difficult to reconcile with known values of moderate (≤50%) extension and the discovery that rapid slip on normal faults began ca. 17 Ma, tens of millions of years after crustal thickening. Here we integrate new and existing stable isotope data, geochronology, and geologic mapping across northeast Nevada that together suggest that the "ignimbrite flareup" magmatism that swept south across the Great Basin ca. 45–20 Ma produced elevated topography supported by normal-thickness crust (mean ~45–50 km). Migrating magmatism progressively shifted the continental divide east into central Nevada from its Late Cretaceous location along the axis of the Sierra arc. This N–S-trending divide developed across broad, dynamic highlands that may have persisted until rapid Basin and Range extension began in middle Miocene time, long after the end of crustal thickening. Extension resulting from spreading of thermally uplifted and weakened crust initiated following removal of the flat-subducting Farallon slab and heating of the crust during mantle-derived magmatism, likely during development of transtensional kinematics along the developing San Andreas plate boundary.

PLAIN LANGUAGE SUMMARY

Although the western USA is one of the world's best-mapped geologic systems, there is considerable uncertainty about how its landscape developed. It is thought that Nevada, eastern California, southern Idaho, and western Utah had high topography (3 km or more) and thick crust (60 km or more) beginning more than 80 million years ago. However, there is little agreement about the actual thickness of the crust, the height of topography, whether topography was a broad plateau or rugged mountains, and when the region spread apart to form today's distinctive basin-and-range topography. We address these questions using stratigraphic studies, stable isotope analyses, and precise mineral ages for sediments from a key area in northeast Nevada. Integrated with prior studies, we are able to show that this region was a broad plateau east of the Sierra Nevada until 45 million years ago. At that time, intense, southward-migrating volcanism reached northeast Nevada, markedly raising elevations. Uplift propagated south with volcanism, progressively shifting the continental divide east into central Nevada. Eventual basin-

and-range spreading was caused by “collapse” of crust that remained hot, high, and weak. Other scientists have shown that spreading finally began 17 million years ago because of changing plate tectonic conditions.

1 INTRODUCTION

The transition from Mesozoic shortening to Cenozoic extension in the western USA Cordillera is a fundamental tectonic switch whose causes are poorly understood. The assortment of models focusing on this time interval reveal underlying disagreements about the pre-extensional crustal structure and topographic character of this region as well as the lithosphere-scale mechanical factors responsible for their change over time. The prevailing view argues that Mesozoic crustal thickening in the Sevier fold and thrust belt produced a high plateau (the “*Nevadaplano*”) across the region of the present-day Great Basin (Fig. 1) (DeCelles, 2004). Although the concept of the *Nevadaplano* is widely accepted, there is significant disagreement regarding the timing and cause of plateau uplift (c.f. Parsons et al., 1994; Mix et al., 2011; Cassel et al., 2018), its peak elevation (c.f. Chase et al., 1998; Wolfe et al., 1998; Best et al., 2009; Cassel et al., 2012), whether and where “rugged topography” may have been present (c.f. Chamberlain et al., 2007; Henry et al., 2012; Snell et al., 2014; Bahadori et al., 2018), and the causes and timing of its inferred “collapse” (c.f. Sonder et al., 1987; McQuarrie and Chase, 2000; Colgan and Henry, 2009; Long, 2012; Wells et al., 2012; Lee et al., 2017).

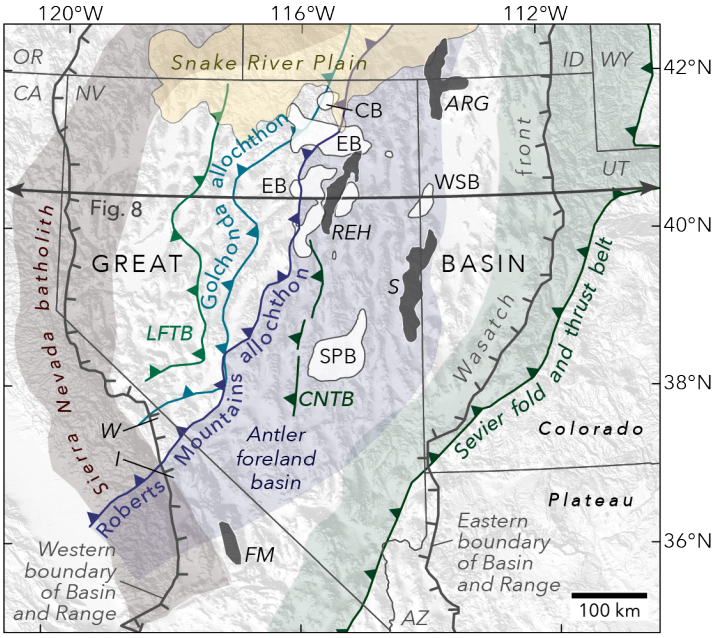

Figure 1. Map of the Great Basin, including the northern and central Basin and Range province (BRP), western USA. The Mesozoic Sierra Nevada batholith is after Van Buer and Miller (2010). Paleogene basins are compiled from Haynes (2003) and Smith et al. (2017). The location of the Luning-Fencemaker thrust belt is from Best et al. (2009). Locations of the Golconda allochthon, Roberts Mountains allochthon, Central Nevada thrust belt, and Sevier fold and thrust belt are from DeCelles (2004). BRP boundary is from Dickinson (2013). ARG = Albion–Raft River–Grouse Creek Mountains; CB = Copper Basin; CNTB = Central Nevada thrust belt; EB = Elko Basin; FM = Funeral Mountains; LFTB = Luning-Fencemaker thrust belt; REH = Ruby Mountains–East Humboldt Range; S = Snake Range; SB = Sheep Pass Basin, WSB = White Sage Basin.

There is general agreement about the location of the late Eocene to earliest Miocene ~N–S regional paleodivide, which is based on the pattern of Cenozoic ash-flow tuffs that filled paleovalleys (e.g., Best et al., 2013; Henry and John, 2013). However, it has not been clearly established how and why the divide shifted eastward into central Nevada from its inferred Late Cretaceous position along the axis of the Mesozoic Sierra Nevada arc (e.g., Van Buer et al., 2009), nor how the topography of western North America might have been affected by the addition of large volumes of magma and heat associated with southward-sweeping (Fig. 2) Cenozoic volcanism (the “ignimbrite flareup” of, e.g., Armstrong and Ward, 1991). Establishing the nature and temporal evolution of these factors and their relationship to faulting and topography are critical to better understanding the transition from shortening to extension across the Cordillera.

To address these questions, we collected additional data from a series of unusually complete and well-studied stratigraphic sections exposed in the region of the former Elko Basin, northeast Nevada. The studied rocks span the latest Mesozoic to Cenozoic transition and record the history of topography changes, the timing of magmatism and faulting leading to crustal extension (Fig. 3). Because Late Cretaceous and Paleogene sedimentary rocks are rare across the Great Basin (Stewart, 1980), strata from this area have been targeted by numerous studies employing geologic mapping (e.g., Haynes, 2003; Lund Snee et al., 2016) and stable isotopes (Horton et al., 2004; Mix et al., 2011; Chamberlain et al., 2012; Feng et al., 2013; Mulch et al., 2015; Smith et al., 2017; Cassel et al., 2018) to evaluate regional tectonism, magmatism, paleoelevation, and paleoclimate. Lund Snee et al. (2016) showed that ages previously assigned to parts of these studied sections were incorrect, demonstrating a need to improve age control on these deposits in order to reevaluate their attendant implications for faulting and topographic changes. As part of the present study, we have refined existing geologic mapping along these key sections (Fig. 4) and used U-Pb detrital zircon geochronology to more precisely link stratigraphic sections and intervals to previously published studies and age constraints. We have also obtained $\delta^{18}O$ stable isotopic measurements to fill the identified gaps in the existing record. We first present the analytical methodology and results and then we outline the implications of the data for the region's tectonic, magmatic, and topographic history.

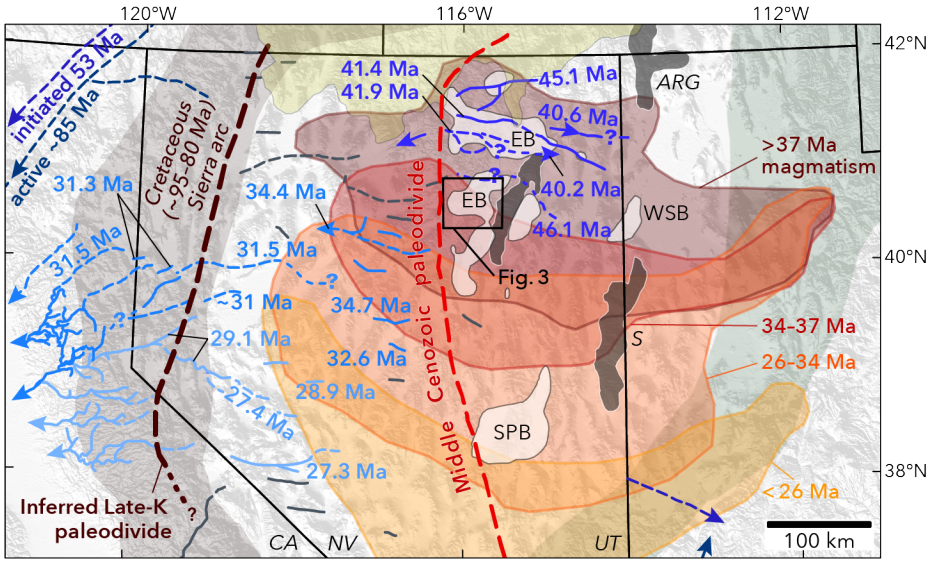

Figure 2. Late Cretaceous and Cenozoic evolution of volcanism, major drainages, and topography in the Great Basin and nearby areas. The approximate location of the Late Cretaceous paleodivide is inferred from Van Buer et al.

(2009) and Sharman et al. (2015). The Cenozoic paleodivide is from Henry and John (2013) and represents the conventional view that the drainage divide was broadly static over Eocene–Oligocene time. Blue paleodrainages are colored by the age of the oldest reported Cenozoic volcanic material deposited within them, compiled from sources given in the Supplementary Information. Lighter blues represent younger paleodrainages, and gray indicates no age information. Volcanic fields are based on data from the North American Volcanic and Intrusive Rock Database (NAVDAT; http://ecp.iedadata.org). Other references and acronyms as in Fig. 1.

2 Geologic setting

The Cenozoic strata that we studied unconformably overlie a thick Triassic to Precambrian section of strata deposited along the passive margin of western North America that was formed by Neoproterozoic to Cambrian rifting of the Rodinia supercontinent (e.g., Lund, 2008). To the west lie older allochthonous deep water rocks of the Roberts Mountains and Golconda allochthons (Fig. 1) that were thrust over the continental margin in the earliest Mississippian and the Permo-Triassic (Stewart, 1980). It is inferred that western Nevada was underlain by oceanic crust and the passive margin succession further east was underlain by thinned continental crust (Tosdal et al., 2000). By the early Triassic, east-dipping subduction was established along the Cordilleran margin (e.g., Saleeby et al., 2008). After this time, the study area lay in the retro-arc region of the evolving Sierra Nevada arc and experienced two general episodes of crustal shortening and metamorphism during periods of increased arc magmatism, one in the Middle to Late Jurassic and the next in the Late Cretaceous ca. 120–70 Ma (Miller and Gans, 1989; Smith et al., 1993; Du Bray, 2007). Late Cretaceous thrust faulting at the latitudes of northern and central Nevada was confined mostly to the Sevier fold and thrust belt to the east of the study area, with significantly less shortening represented by the Central Nevada thrust belt (Taylor et al., 2000) in central and southern Nevada (Fig. 1). Following Sevier shortening, the Cordilleran orogen at these latitudes transitioned to a state of extension. It remains controversial whether extension initiated as early as Eocene or even Late Cretaceous time in certain areas (e.g., Henry et al., 2011; Miller et al., 2012; Wells et al., 2012), but it is clear that rapid ~WNW–ESE Basin and Range extension initiated only in middle Miocene time (Lund et al., 1993; Miller et al., 1999; Henry, 2008; Colgan and Henry, 2009; Colgan et al., 2010; Colgan, 2013; Konstantinou and Miller, 2015; Lund Snee et al., 2016). The main episode of extension in the Great Basin (northern BRP) occurred long after an episode of intense, widespread “ignimbrite flare-up” volcanism and plutonism that swept south-southwest from southern Canada to the latitudes of

Las Vegas in early and middle Cenozoic time (Armstrong, 1970; Dickinson, 2013; Konstantinou and Miller, 2015), passing through the Great Basin (Fig. 2) between ca. 44–20 Ma (Brooks et al., 1995; Ressel and Henry, 2006; Ryskamp et al., 2008; Henry and John, 2013; Lund Snee et al., 2016).

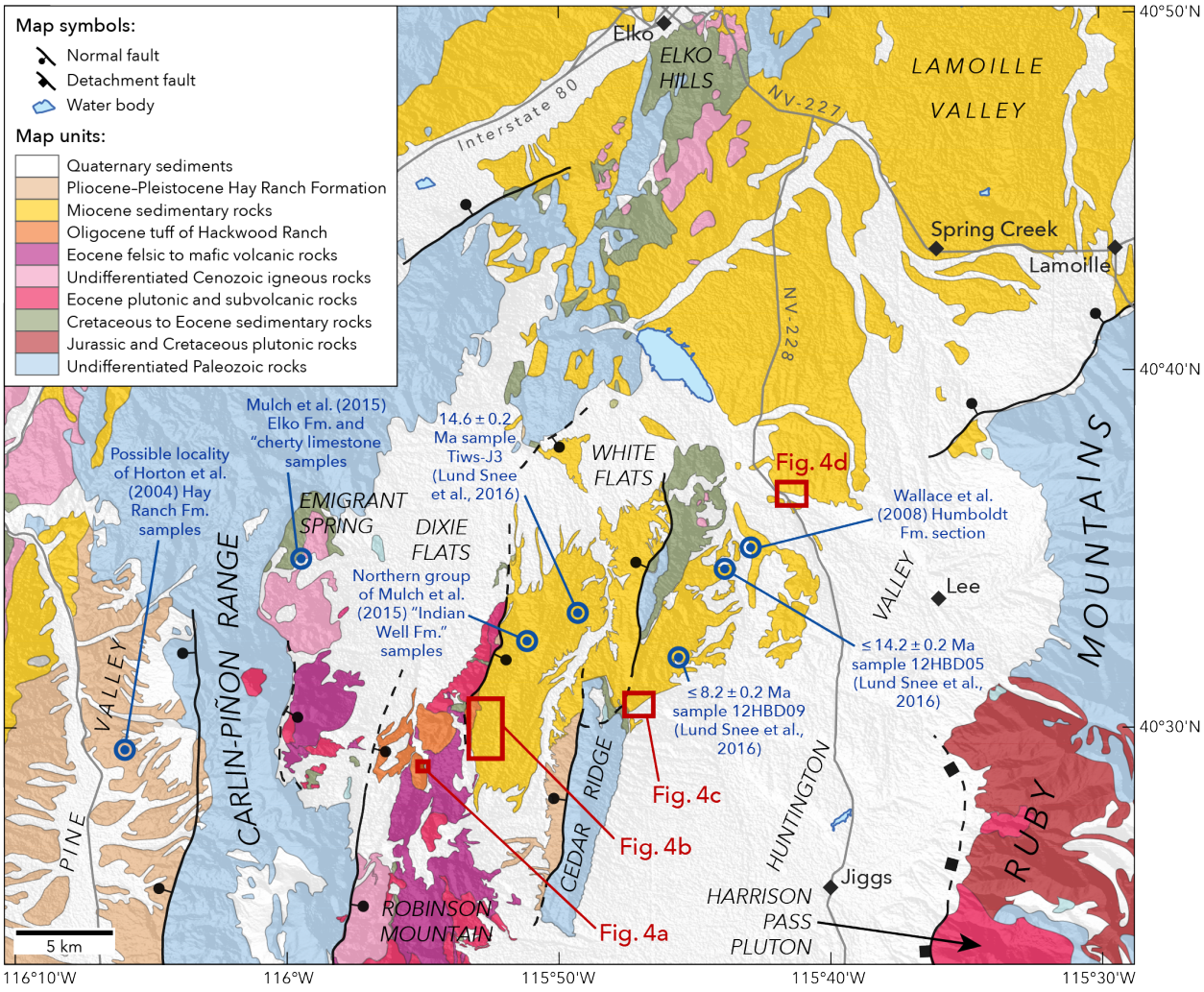

Figure 3. Geologic map of the greater Elko Basin region, northeast Nevada (location shown in Fig. 2). Unit boundaries and faults are from Crafford (2007), Colgan et al. (2010), Lund Snee et al. (2016), and this study.

In many areas, Cenozoic south-sweeping magmatism added 1 km or more of volcanic material to the Earth's surface (Gans et al., 1989; Best et al., 2009; Henry and John, 2013), and likely several times more plutonic material (Gans, 1987; Lachenbruch and Morgan, 1990; Catchings and Mooney, 1991). This magmatism was ultimately mantle-derived and its sources were related to asthenospheric upwelling resulting from foundering of the inferred flat-subducting Farallon slab, which led to melting of subduction-hydrated and metasomatized sub-

continental mantle (Armstrong and Ward, 1991; Humphreys, 1995). Miocene extension across the northern BRP (Great Basin) began along the center and eastern part of the present province and then affected crust successively further west and north (Stockli et al., 2002; Surpless et al., 2002; Stockli, 2005; Colgan et al., 2006). The Humboldt Formation (Sharp, 1939), which is predominantly middle to late Miocene in age, forms thick deposits in the study area (Fig. 3) and provides the primary sedimentary record of rapid fault slip, half-graben basin formation and extension in northeast Nevada (Wallace et al., 2008; Colgan et al., 2010; Lund Snee et al., 2016).

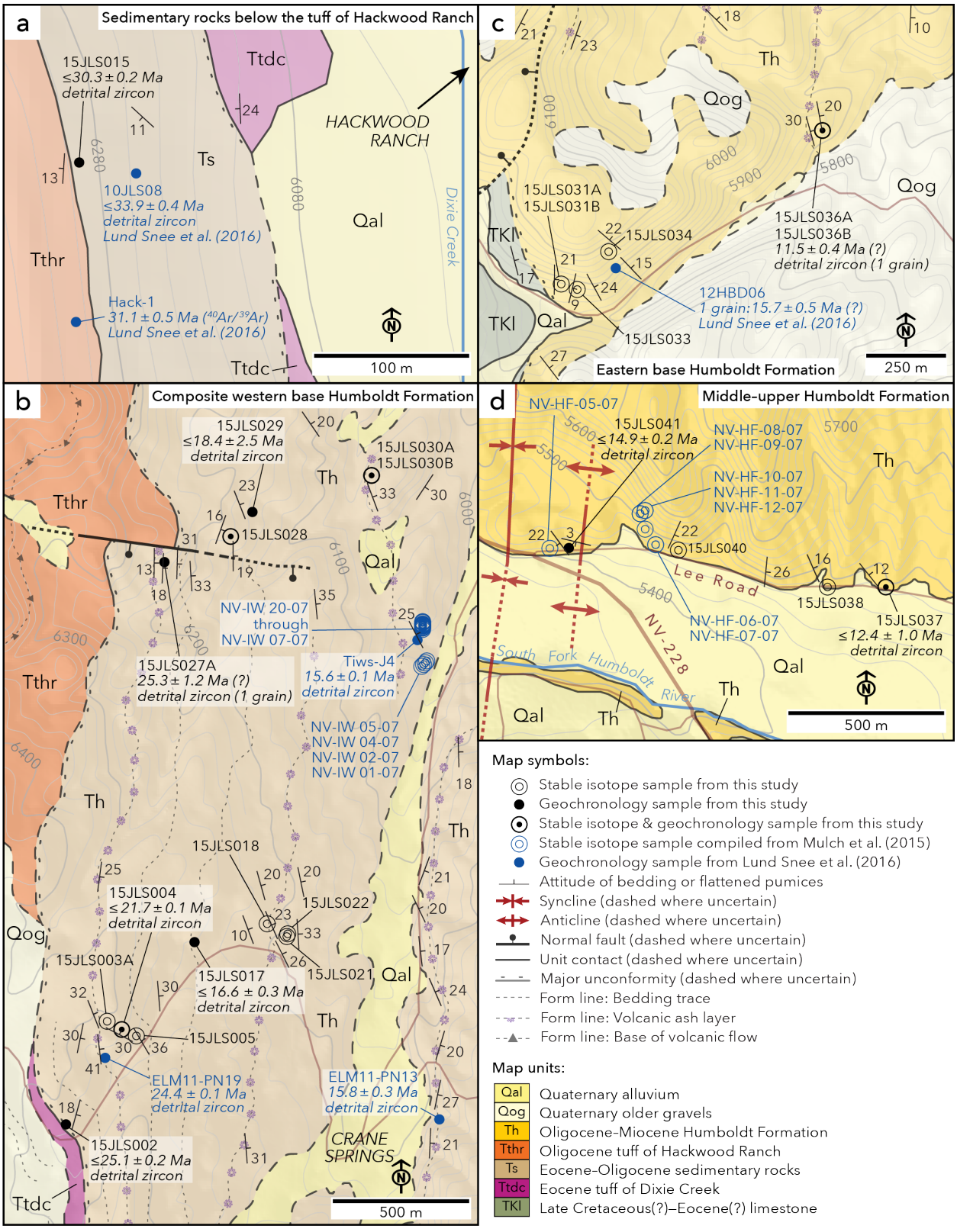
a
Sedimentary rocks below the tuff of Hackwood Ranch
15JLS015
≤30.3 ± 0.2 Ma
detrital zircon
10JLS08
≤33.9 ± 0.4 Ma
detrital zircon
Lund Snee et al. (2016)
Hack-1
31.1 ± 0.5 Ma (40Ar/39Ar)
Lund Snee et al. (2016)
Ttdc
Ts
Tthr
Qal
HACKWOOD RANCH
Dixie Creek
100 m
b
Composite western base Humboldt Formation
15JLS029
≤18.4 ± 2.5 Ma
detrital zircon
15JLS030A
15JLS030B
15JLS028
15JLS027A
25.3 ± 1.2 Ma (?)
detrital zircon (1 grain)
NV-IW 20-07
through
NV-IW 07-07
Tiws-J4
15.6 ± 0.1 Ma
detrital zircon
NV-IW 05-07
NV-IW 04-07
NV-IW 02-07
NV-IW 01-07
15JLS018
15JLS004
≤ 21.7 ± 0.1 Ma
detrital zircon
15JLS022
15JLS003A
15JLS017
≤ 16.6 ± 0.3 Ma
detrital zircon
15JLS021
15JLS005
ELM11-PN19
24.4 ± 0.1 Ma
detrital zircon
ELM11-PN13
15.8 ± 0.3 Ma
detrital zircon
15JLS002
≤25.1 ± 0.2 Ma
detrital zircon
CRANE SPRINGS
Th
Tthr
Qal
Qog
Ttdc
500 m
c
Eastern base Humboldt Formation
15JLS031A
15JLS031B
15JLS034
15JLS036A
15JLS036B
11.5 ± 0.4 Ma (?)
detrital zircon (1 grain)
12HBD06
1 grain: 15.7 ± 0.5 Ma (?)
Lund Snee et al. (2016)
15JLS033
TKl
Qal
Qog
Th
250 m
d
Middle-upper Humboldt Formation
NV-HF-05-07
15JLS041
≤14.9 ± 0.2 Ma
detrital zircon
NV-HF-08-07
NV-HF-09-07
NV-HF-10-07
NV-HF-11-07
NV-HF-12-07
15JLS040
15JLS038
15JLS037
≤12.4 ± 1.0 Ma
detrital zircon
NV-HF-06-07
NV-HF-07-07
Lee Road
NV-228
South Fork Humboldt River
Th
Qal
500 m
Map symbols:
Stable isotope sample from this study
Geochronology sample from this study
Stable isotope & geochronology sample from this study
Stable isotope sample compiled from Mulch et al. (2015)
Geochronology sample from Lund Snee et al. (2016)
Attitude of bedding or flattened pumices
Syncline (dashed where uncertain)
Anticline (dashed where uncertain)
Normal fault (dashed where uncertain)
Unit contact (dashed where uncertain)
Major unconformity (dashed where uncertain)
Form line: Bedding trace
Form line: Volcanic ash layer
Form line: Base of volcanic flow
Map units:
Qal Quaternary alluvium
Qog Quaternary older gravels
Th Oligocene-Miocene Humboldt Formation
Tthr Oligocene tuff of Hackwood Ranch
Ts Eocene-Oligocene sedimentary rocks
Ttdc Eocene tuff of Dixie Creek
TKl Late Cretaceous(?)–Eocene(?) limestone

Figure 4. Geologic maps of areas sampled for this study. Unit boundaries and structures are from Smith and Howard (1977), Crafford (2007), Lund Snee et al. (2016), and this study. Maximum depositional ages are indicated with inequality symbols ("≤"), unlike for nearly absolute depositional ages from tuffaceous horizons.

3 METHODS

We report U-Pb detrital zircon ages for 9 new samples and 67 measurements of $\delta^{18}O$ and $\delta^{13}C$ from 20 sedimentary samples collected in the Elko Basin area (Fig. 3). This study expands upon and refines geologic mapping by Smith and Howard (1977), Smith and Ketner (1978), Lund Snee (2013), Lund Snee and Miller (2015), and Lund Snee et al. (2016), who provided detailed descriptions of those rocks and (re-)assigned ages throughout the stratigraphic succession.

Stable isotope and age data compiled here from this and prior studies (Horton et al., 2004; Mix et al., 2011; Chamberlain et al., 2012; Mulch et al., 2015) in the Elko Basin are from the Eocene Elko Formation, the latest Oligocene to late Miocene Humboldt Formation, and the middle Pliocene–middle Pleistocene Hay Ranch Formation (Fig. 3). Rocks described by those studies as belonging to the Eocene–Oligocene Indian Well Formation were found by Lund Snee et al. (2016) to belong to the younger Humboldt Formation and thus the Indian Well Formation is no longer used for these strata. Here we apply improved age constraints for the rocks from all of the units sampled by the prior studies using both the new U-Pb geochronologic constraints and previously published age information. Sample localities are indicated in Fig. 4 and their stratigraphic position and associated age constraints are shown in Fig. 5.

The rocks we analyzed for $\delta^{18}O$ values were mostly obtained from the latest Oligocene to late Miocene Humboldt Formation, which was mapped and described in detail by Lund Snee (2013) and Lund Snee and Miller (2015). We have focused on improving age constraints and expanding the sample database to cover higher and lower parts of the sections, in order to provide a more complete description of the basin history. The rocks sampled include limestones, marls, shales, and sandstones, which were typically carbonate cemented and often contained appreciable volcanic ash material as well. Tables S1 and S4 provide the lithologic details for each sample, together with sample localities, (maximum) depositional age information, and analytical data. Rocks sampled from a localized, unnamed sedimentary unit (Ts) immediately below the ca. 31.1 Ma tuff of Hackwood Ranch (Figs. 4a and 5) yielded insufficient carbonate to obtain reliable $\delta^{18}O$ values.

202

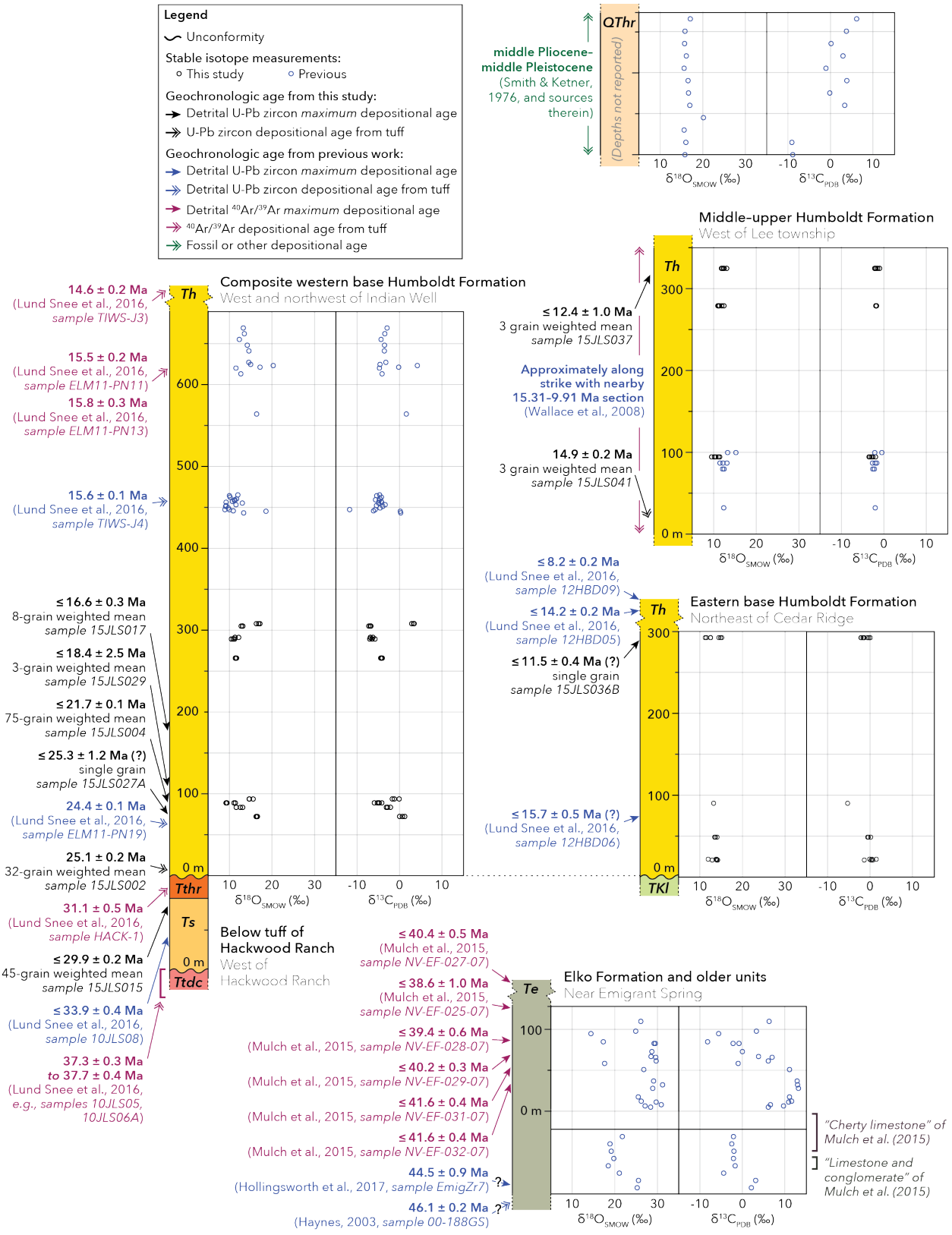
Legend
Unconformity
Stable isotope measurements:
This study
Previous
Geochronologic age from this study:
Detrital U-Pb zircon maximum depositional age
U-Pb zircon depositional age from tuff
Geochronologic age from previous work:
Detrital U-Pb zircon maximum depositional age
Detrital U-Pb zircon depositional age from tuff
Detrital 40Ar/39Ar maximum depositional age
40Ar/39Ar depositional age from tuff
Fossil or other depositional age
QThr
(Depths not reported)
middle Pliocene–middle Pleistocene (Smith & Ketner, 1976, and sources therein)
δ18OSMOW (‰)
δ13CPDB (‰)
Middle-upper Humboldt Formation
West of Lee township
Th
≤ 12.4 ± 1.0 Ma
3 grain weighted mean
sample 15JLS037
Approximately along strike with nearby 15.31–9.91 Ma section (Wallace et al., 2008)
14.9 ± 0.2 Ma
3 grain weighted mean
sample 15JLS041
Composite western base Humboldt Formation
West and northwest of Indian Well
14.6 ± 0.2 Ma (Lund Snee et al., 2016, sample TIWS-J3)
15.5 ± 0.2 Ma (Lund Snee et al., 2016, sample ELM11-PN11)
15.8 ± 0.3 Ma (Lund Snee et al., 2016, sample ELM11-PN13)
15.6 ± 0.1 Ma (Lund Snee et al., 2016, sample TIWS-J4)
≤ 16.6 ± 0.3 Ma
8-grain weighted mean
sample 15JLS017
≤ 18.4 ± 2.5 Ma
3-grain weighted mean
sample 15JLS029
≤ 21.7 ± 0.1 Ma
75-grain weighted mean
sample 15JLS004
≤ 25.3 ± 1.2 Ma (?)
single grain
sample 15JLS027A
24.4 ± 0.1 Ma (Lund Snee et al., 2016, sample ELM11-PN19)
25.1 ± 0.2 Ma
32-grain weighted mean
sample 15JLS002
Tthr
31.1 ± 0.5 Ma (Lund Snee et al., 2016, sample HACK-1)
Ts
≤ 29.9 ± 0.2 Ma
45-grain weighted mean
sample 15JLS015
Ttdc
≤ 33.9 ± 0.4 Ma (Lund Snee et al., 2016, sample 10JLS08)
37.3 ± 0.3 Ma to 37.7 ± 0.4 Ma (Lund Snee et al., 2016, e.g., samples 10JLS05, 10JLS06A)
≤ 8.2 ± 0.2 Ma (Lund Snee et al., 2016, sample 12HBD09)
≤ 14.2 ± 0.2 Ma (Lund Snee et al., 2016, sample 12HBD05)
≤ 11.5 ± 0.4 Ma (?)
single grain
sample 15JLS036B
Eastern base Humboldt Formation
Northeast of Cedar Ridge
≤ 15.7 ± 0.5 Ma (?) (Lund Snee et al., 2016, sample 12HBD06)
TKl
Below tuff of Hackwood Ranch
West of Hackwood Ranch
≤ 40.4 ± 0.5 Ma (Mulch et al., 2015, sample NV-EF-027-07)
≤ 38.6 ± 1.0 Ma (Mulch et al., 2015, sample NV-EF-025-07)
≤ 39.4 ± 0.6 Ma (Mulch et al., 2015, sample NV-EF-028-07)
≤ 40.2 ± 0.3 Ma (Mulch et al., 2015, sample NV-EF-029-07)
≤ 41.6 ± 0.4 Ma (Mulch et al., 2015, sample NV-EF-031-07)
≤ 41.6 ± 0.4 Ma (Mulch et al., 2015, sample NV-EF-032-07)
44.5 ± 0.9 Ma (Hollingsworth et al., 2017, sample EmigZr7) ?
46.1 ± 0.2 Ma (Haynes, 2003, sample 00-188GS) ?
Elko Formation and older units
Near Emigrant Spring
Te
"Cherty limestone" of Mulch et al. (2015)
"Limestone and conglomerate" of Mulch et al. (2015)

203

Figure 5. Plots of isotopic analyses by stratigraphic section. Section and sample locations are shown in Fig. 4. Maximum depositional ages are indicated with inequality symbols ("≤"), unlike for nearly absolute depositional ages from tuffaceous horizons. Plotted stable isotope measurements and age data are listed in the Supplementary Information. These plots complement those in Fig. 6, where isotopic measurements from all stratigraphic sections are plotted together by preferred depositional age.

3.1 Methods for U-Pb detrital zircon geochronology

Mineral separation and analytical procedures for U-Pb detrital zircon geochronology closely followed those by Dumitru et al. (2016). Fresh, fine-grained samples were sought and weathered rinds were removed. Samples were crushed and mineral separates were made at Stanford University using standard magnetic and gravity techniques. Zircon grains were dump-mounted to avoid biasing in the analysis of grains. For tuffaceous samples, euhedral grains were not analyzed separately as reworking can abrade grains. Samples were analyzed by the laser ablation inductively coupled mass spectrometer (LA–ICP–MS) method. A first group of samples was analyzed at the University of California, Santa Cruz (UCSC), Institute of Marine Sciences. Another group was analyzed at the University of Arizona LaserChron Center following procedures of Gehrels et al. (2006, 2008). For samples analyzed at UCSC, data reduction was conducted with the Iolite v.2.5 add-in to IGOR Pro v.6.3 (Paton et al., 2011) using the "U_Pb_Geochronology3" data reduction scheme. For both groups, final data analysis was performed using Isoplot v.3.75 (Ludwig, 2008). The reported ages are from the $^{206}Pb/^{238}U$ system for $^{206}Pb/^{238}U$ ages < 1000 Ma and otherwise from the $^{207}Pb/^{206}Pb$ system. For grains with $^{206}Pb/^{238}U$ ages > 800 Ma, grains were excluded in cases of discordance > 30% or < –7% relative to $^{207}Pb/^{206}Pb$ ages. Please see the Supplementary Information for additional details.

3.2 Methods for assigning (maximum) depositional ages

As illustrated in Fig. 5, three techniques were applied to determine depositional age constraints for the strata sampled for stable isotope values, depending on the types of rocks and available age data. The youngest isotopically dated mineral population within a detrital sample provides a maximum depositional age (MDA). Second, fossil ages (from previous studies) provide age brackets for all or part of a stratigraphic unit. Third, isotopic dating or tephra correlation conducted on volcanic minerals within air- or water-lain tuffs can, in some cases, provide absolute depositional ages. Although it is possible that such tuffs experienced some

reworking by fluvial or lacustrine processes, their eruption ages are likely close to the time of deposition (probably << 1 Ma). This is supported by the large number of temporally distinct Cenozoic tuffs preserved in basins across the northern Basin and Range Province, often with short gaps between subsequent eruptions, all of which typically provide tight temporal constraints on depositional ages (Wallace et al., 2008). In particular, Neogene silicic tuffs erupted from the Snake River Plain (Fig. 1) provide excellent and high-resolution age control for basin-and-range faulting and sediment deposition throughout this region. Faulting began approximately at the onset of silicic eruptions ca. 16.5 Ma (Coble and Mahood, 2012), rapidly creating accommodation space for sediments in fault hanging walls. Silicic eruptions occurred frequently along the SRP from its inception ca 16.5 to the present. For these reasons, any volcanic material that spent large amounts of time being reworked at the surface would have a high probability of including material from younger eruptions.

For isotopically dated samples, maximum and absolute depositional ages from sedimentary rocks and tuffs were determined by estimating the weighted mean of the youngest coherent group of ages (Fig. S2). In several cases, the youngest coherent group was straightforwardly identified as those whose ages overlapped within 2σ uncertainty and were clearly younger than others (outside the 2σ error bounds). In less clear cases, the youngest coherent group was determined in an interpretive fashion that attempted to maximize the number of included grains while avoiding inclusion of so many grains as to significantly increase age uncertainty. All but one of such cases yielded mean square weighted deviation (MSWD) ~1.0. That case (sample 15JLS002; Fig. S2b) yielded MSWD = 0.42 because of several relatively young grains, but the age that would produce MSWD = 1 is also shown.

Data from the 5 stratigraphic sections shown in Fig. 6 are compiled together into a generalized column based on the preferred depositional ages listed in Tables S3 and S4. The preferred ages for samples analyzed for stable isotope values (which do not all have isotopic ages) were assigned by assuming constant sedimentation rates between horizons with age constraints as shown in Fig. 5, although we are aware that constant deposition was unlikely. Vertical error bars in Fig. 6 indicate the full range of permissible ages for individual analyses between minimum and maximum age brackets, conservatively incorporating the 2σ age uncertainties.

3.3 Methods for sampling and stable isotope measurements

When sampling sedimentary rocks for stable isotope analysis, we chose samples that appeared to have high authigenic calcite content on the basis of outcrop appearance or effervescence upon exposure to 10% HCl. We sought unexposed material by digging and trenching and we removed any weathering rinds using a rock hammer. We removed all possible dust from samples in the field and then again in the laboratory using compressed air to reduce any potential for contamination. Throughout the Humboldt Formation, water-lain, weakly bedded tephra beds are interlayered between clastic lacustrine carbonates (marls), siliciclastic fine- and medium-grained fluvial (typically cross-bedded) sandstones, and thin (generally <1 m) pebble conglomerates (Lund Snee et al., 2016). Sampled rocks range from marls to often calcite cemented fine- and medium-grained fluvial sandstones. Some of the earlier sampled strata from the lower Humboldt Formation (previously called the Indian Well Formation) reportedly included paleosols (Mulch et al., 2015). Ash or other volcanic material is present in most Humboldt Formation strata, and calcite cement comprises the authigenic carbonate.

We obtained powder from carbonate-rich samples using ~0.5–2.0 mm width bits fastened to a Dremel tool. Sampled spot locations were selected for their likelihood of containing calcite cement or matrix. While care was taken to sample only matrix material, we cannot exclude the possibility that sampling included small amounts of detrital carbonates, silicates, volcanic rock fragments, and other materials in addition to matrix material. Accordingly, subsamples were obtained and analyzed in triplicate or quintuplicate for each sample to ensure redundancy and to reduce the effect of bias from incorporation of detrital carbonates.

The carbon and oxygen isotope values of carbonates were obtained at the Stable Isotope Biogeochemistry Laboratory, Stanford University, using a Thermo Finnigan Gasbench interfaced with a Thermo Finnigan Delta Plus XL mass spectrometer. Between 0.3 and 4.8 mg of carbonate powder (typically about 0.5 mg) was weighed into sealed vials that were flushed with He gas and reacted with ~0.5 ml of phosphoric acid (H_3PO_4) for 1 hour at 72º C. External precision (1σ) of oxygen and carbon isotope data is ≤0.08‰, based upon repeated measurements of two internal lab reference materials (calibrated against NBS 18, NBS 19, and LSVEC). The samples were analyzed in three sessions: 26 April 2016, 8 July 2016, and 9 July 2016. Analyses were excluded from the first session if weight percent carbonate was <24. All $\delta^{13}C$ values are reported relative to VPDB and $\delta^{18}O$ values are reported relative to VSMOW. Table S3 lists the stratigraphic

position, inferred ages, stable isotope results, and analytical details for stable isotope measurements.

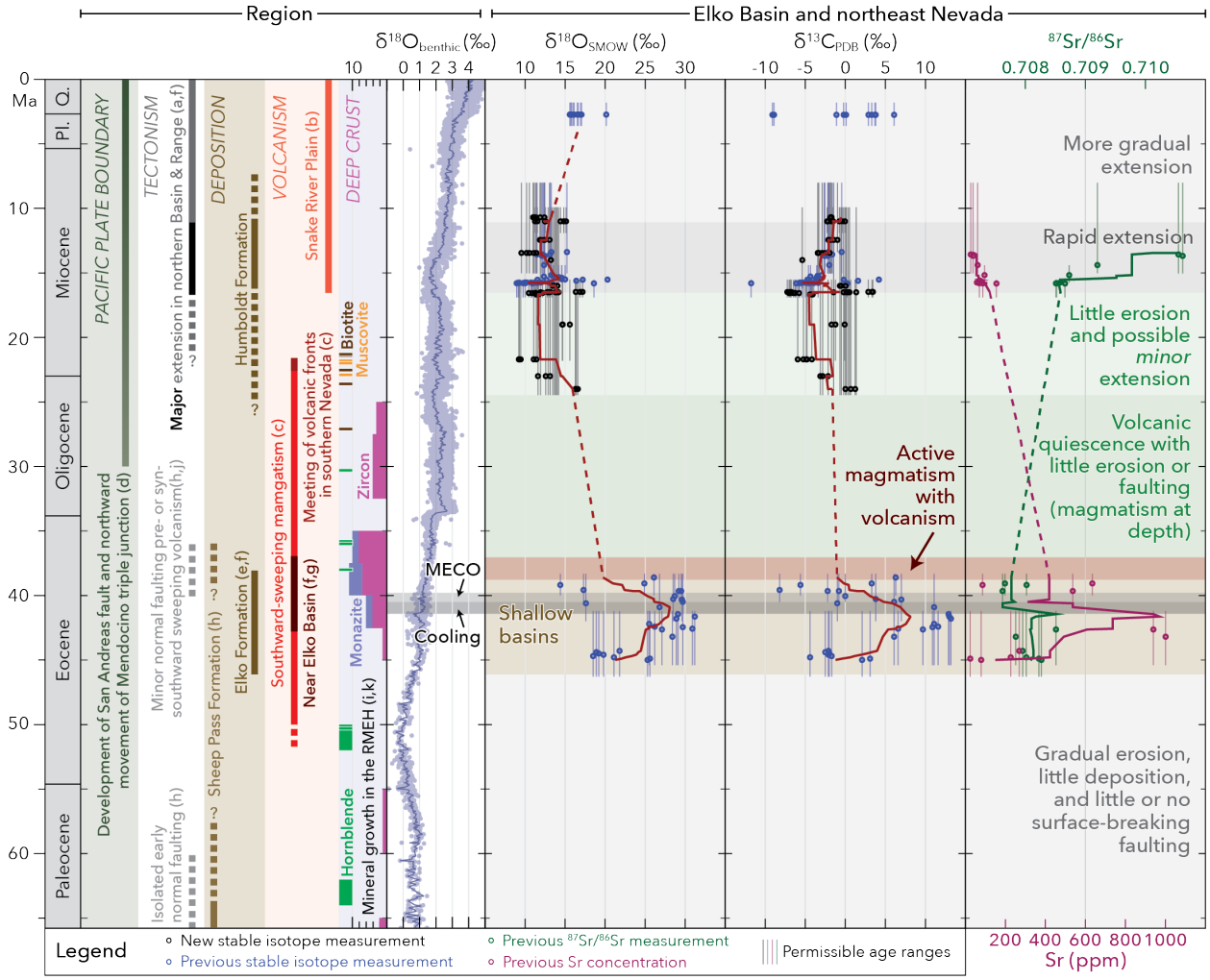

Figure 6. Composite chart of regional Cenozoic tectonic events and measured isotopic values in the eastern Piñon Range and central Huntington Valley. Stable isotope and Sr data are from this study, Horton et al. (2004), Mix et al. (2011), Chamberlain et al. (2012), and Mulch et al. (2015). Vertical bars indicate the full permissible age range for each analysis, conservatively including the 2σ uncertainties of the bounding age constraints. Stable isotope value uncertainties are too small to be visible. Benthic $\delta^{18}O$ values are from Zachos et al. (2001). References: a—Colgan and Henry (2009); b—Coble and Mahood (2012); c—Armstrong and Ward (1991); d—Atwater (1989); e—Haynes (2003); f—Lund Snee et al. (2016); g—Brooks et al. (1995); h—Druschke et al. (2009a); i—Howard et al. (2011); j—Henry et al. (2011); and k—McGrew and Snee (1994).

4 RESULTS

4.1 Results of U-Pb detrital zircon geochronology

A sandstone sample (15JLS015) collected from near the top of a thin (<200 m) sedimentary deposit below the tuff of Hackwood Ranch (Fig. 4a) yielded an MDA of 29.9 ± 0.2 Ma on the basis of the weighted mean of 45 analyses (Fig. 5). Lund Snee et al. (2016) obtained a U-Pb detrital zircon MDA of 33.9 ± 0.4 Ma from a sample (10JLS08) collected nearby but stratigraphically lower within the same unit. The age of these deposits is bracketed below by a U-Pb SHRIMP (zircon) age of 37.34 ± 0.33 Ma (sample 10JLS05) from the tuff of Dixie Creek and above by a $^{40}Ar/^{39}Ar$ (sanidine) age of 31.10 ± 0.47 Ma on the tuff of Hackwood Ranch (Lund Snee et al., 2016). It is unclear why the detrital zircon age of sample 15JLS015 is ≥0.5 Ma younger than the previously obtained $^{40}Ar/^{39}Ar$ age of the overlying tuff (counting error), but we take the tuff age to be authoritative because multiple samples and isotopic systems have yielded consistent ages (see Lund Snee et al., 2016).

The remaining detrital zircon ages were obtained for samples collected from the latest Oligocene–Miocene Humboldt Formation. Deposition of the Humboldt Formation was previously bracketed to ca. 24.4 ± 0.1 Ma (U-Pb zircon sample ELM11-PN19) at the bottom to at least 8.2 ± 0.2 Ma (U-Pb zircon sample 12HBD09) at the top (Lund Snee et al., 2016). A tuffaceous sandstone from the western measured sections (Figs. 3 and 4b) representing the stratigraphically lowest Humboldt Formation sample that was analyzed as part of this study (15JLS002, 5 m above the angular unconformity with underlying Eocene and Oligocene tuffs) extends the oldest known MDA of this unit to 25.1 ± 0.2 Ma (a weighted mean of 32 grains). Progressing stratigraphically upward in the western section, a pebble conglomerate (sample 15JLS027A, 72 m stratigraphic height) provided a tentative MDA of 25.3 ± 1.2 Ma, on the basis of a single young grain. Because this age is older than those of the underlying strata (Fig. 5), it did not contribute to constraining depositional ages. An overlying pebble conglomerate with an ashy matrix (sample 15JLS004; 89 m) yielded a younger MDA of 21.7 ± 0.1 Ma on the basis of a 75-grain weighted mean. One younger grain (15.7 ± 0.9 Ma) was excluded from this analysis due to obvious zoning; it is therefore possible that this sample could be ca. 16 Ma or younger, although the sample's stratigraphic position near and below samples containing only significantly older ages discounts this possibility. Slightly above (101 m), a weighted mean of 3 analyses established an MDA of 18.4 ± 2.5 Ma for a matrix-supported pebble conglomerate (sample 15JLS029). Finally, an ashy sandstone (15JLS017) yielded a younger MDA of 16.6 ± 0.3 Ma from 8 grains. Four previously published approximately absolute depositional ages

from tuffs higher in this section young progressively upward to ca. 14.6 Ma (Fig. 5) (Lund Snee et al., 2016).

A second Humboldt Formation section was sampled further east (Fig. 4c), across a normal fault with >700 m throw that exposes the base of the Humboldt Formation in its footwall (Wallace et al., 2008; Lund Snee and Miller, 2015; Lund Snee et al., 2016). The currently available ages within this section are not as well constrained as to the west but they represent the available information. At 292 m from the base of the measured section, a single grain at 11.5 ± 0.4 Ma provides a tentative MDA. This relatively young age may be reliable because Lund Snee et al. (2016) reported an older MDA of 15.7 ± 0.5 Ma (also tentative because it was based on a single U-Pb detrital zircon grain) from an underlying sample (12HBD06; 77 m) within this section (Fig. 5). Stratigraphically higher in this area, Lund Snee et al. (2016) reported a U-Pb detrital zircon age of 8.2 ± 0.2 Ma, representing the youngest known MDA of the Humboldt Formation.

A third Humboldt Formation section was sampled to the northeast, west of the Lee township (Fig. 4d), and roughly along strike of a section along Huntington Creek from which Wallace et al., (2008) reported tuff (absolute depositional) ages that decrease upward from 15.31–9.91 Ma. An approximately absolute depositional age of 14.9 ± 0.2 Ma was established based on a 3-grain weighted mean for a tephra sample (15JLS041) collected from the base of the section (0 m). Near the top of this section (325 m), a silty sandstone (sample 15JLS037) yielded an MDA of 12.4 ± 1.0 Ma based on a 3-grain weighted mean.

Fig. 6 illustrates the permissible depositional age ranges and our preferred ages for the samples analyzed for stable isotope values based on these constraints. Preferred ages and bounds were assigned according to the above guidelines. In addition, we improved depositional ages for previously reported stable isotope measurements from the older Cenozoic succession sampled in the Elko Basin area, for which a number of contradictory age ranges were previously reported (c.f. Horton et al., 2004; Mix et al., 2011; Chamberlain et al., 2012; Mulch et al., 2015; Smith et al., 2017). In most cases, the permissible age bounds were not previously given, and sample ages were reported as being absolute when in fact they were MDAs. The new preferred ages and permissible bounds presented here account for changes to age assignments required by this more recent geochronology, as illustrated in Fig. 5 and explained in further detail within the Supplementary Information.

375

376 **4.2 Stable isotope measurements**

377 Stable isotope values reported here are from the latest Oligocene–Miocene Humboldt
378 Formation. Here we describe the observed shifts in stable isotope values within the Cenozoic
379 succession illustrated in Fig. 6, compiled from this and prior work. Within the lower Elko
380 Formation (the oldest strata sampled for stable isotope values in the Elko Basin), $\delta^{18}O$
381 (VSMOW) values are relatively high, increasing from about +19–+26‰ to +25–+31‰ between
382 ca. 45 to 42 Ma. During the same interval, $\delta^{13}C$ (VPDB) values also increase from about –4–+3
383 to > +10‰, and then they decrease significantly in the upper Elko Formation (42–38 Ma), to –8–
384 +6‰. Values of $\delta^{18}O$ also decrease over this latter interval, although data are somewhat scattered
385 and the magnitude of this decrease hinges upon three samples with $\delta^{18}O$ values < 20‰ ca. 41–39
386 Ma (Fig. 6). Regardless, by 24 Ma, $\delta^{18}O$ values had clearly decreased dramatically, to <+17‰.
387 Values of $\delta^{13}C$ also remained relatively low (mostly <+2‰) until well after 24 Ma.

388 Precisely determining the timing of the large negative shift in $\delta^{18}O$ values is complicated
389 by a substantial gap in the record between the end of Elko Formation deposition ca. 38 (Haynes,
390 2003; Lund Snee et al., 2016) and the start of Humboldt Formation deposition ca. 25 Ma. This
391 gap reflects a near-total absence of deposition in the Elko Basin and surrounding areas in
392 Oligocene and early Miocene time, with critical implications for paleotopographic and tectonic
393 evolution (discussed below). Rare exceptions are represented by Oligocene conglomerates in
394 Copper Basin (Henry et al., 2011), north of the Elko Basin (Fig. 1), and by thin Oligocene
395 sedimentary deposits (Ts) below the tuff of Hackwood Ranch in the Elko Basin (Lund Snee and
396 Miller, 2015). Unfortunately, sandstone samples from the Ts unit (Fig. 4a) contained insufficient
397 carbonate content to provide reliable stable isotope measurements. Although Cassel et al. (2014,
398 2018) obtained δD values from rocks younger than 33 Ma elsewhere in the Great Basin, stable
399 isotope values in the Oligocene are undocumented in northeast Nevada due to the lack of
400 sediments of this age. In the study area, the beginning of this gap coincides with the onset of
401 volcanism.

402 Throughout the sampled portion of the Humboldt Formation (ca. 24–10 Ma), $\delta^{18}O$ values
403 remain relatively low, generally varying between +10–+16‰. Over the same interval, $\delta^{13}O$
404 values are generally –7–0‰, with some additional scatter, but they appear to increase slightly in
405 the latter portion of this interval, from about –4 to 0‰ between ca. 16–10 Ma. Subsequently,

between the youngest sampled Humboldt Formation deposits ca. 10 Ma and the potentially middle Pliocene onset of Hay Ranch Formation deposition (Regnier, 1960; Smith et al., 1976), $\delta^{18}O$ values increase moderately to +15–+20‰, whereas $\delta^{13}C$ values are widely scattered between –9–+6‰.

The shifts in $\delta^{18}O$ and $\delta^{13}C$ values are accompanied by changes in $^{87}Sr/^{86}Sr$ and Sr concentration (Mulch et al., 2015). Throughout the Eocene (at least until ca. 38 Ma), $^{87}Sr/^{86}Sr$ values remain relatively low (0.7075–0.7085) but increase slightly to >0.7085 in Middle Miocene time (16 Ma). Subsequently, $^{87}Sr/^{86}Sr$ values increase dramatically to >0.710 by 14 Ma. Over the sampled intervals, Sr concentration followed a similar pattern to $\delta^{18}O$ values, increasing from <200 ppm ca. 45 Ma to ~1000 ppm ca. 42 Ma, then declining moderately to scattered values ranging between ~200–600 ppm, before decreasing dramatically to <200 ppm between ca. 16–14 Ma.

5 DISCUSSION

5.1 Interpretation of stable isotope results

Oxygen stable isotope values measured in authigenic carbonates provide information about a region's hypsometric mean elevation during deposition (Poage and Chamberlain, 2001). Because heavy isotopes (e.g., ^{18}O rather than ^{16}O) are preferentially precipitated as an air mass rises over an orographic barrier, $\delta^{18}O$ can be inversely proportional to the height of the tallest mountain chain between a sampled area and the source of precipitation, providing insights for temporal or spatial changes in paleoelevation. However, other factors also affect preserved isotopic values, notably climate and diagenesis (Blisniuk and Stern, 2005; Ehlers and Poulsen, 2009; Fiorella et al., 2015), so changes in $\delta^{18}O$ often should not be directly interpreted to indicate changes in elevation. In addition, although the Pacific Ocean likely represented the primary moisture source for the Great Basin in Eocene and Oligocene time, some proportion of moisture was also derived from the Gulf of California and Gulf of Mexico, depending in part on the existing topography (Chamberlain et al., 2012). Furthermore, isotopic lapse rates can vary considerably by tectonic setting, and they are known to be especially uncertain in the BRP (Lechler and Niemi, 2011a).

Here we discuss the implications of the changes in stable isotope values in the context of climate and basin fill record. The potential effects of paleoclimate on stable isotope values

recorded in northeast Nevada have been discussed at length (Feng et al., 2013; Mulch et al., 2015; Smith et al., 2017). However, prior interpretations are limited by the discovery that the age assignments applied to most of the same strata were incorrect to varying degrees (Lund Snee et al., 2016). For all of the above reasons, we interpret the changes in $\delta^{18}O$ and $\delta^{13}C$ values shown in Fig. 6 in an intentionally qualitative fashion that incorporates geologic data, pointing out which models and geologic relations are consistent with the measured changes in isotopic values and, in general, the implied changes in elevation.

In the lower parts of the Eocene Elko Formation (the oldest strata that have been sampled for stable isotope values in northeast Nevada) a ~5‰ increase in $\delta^{18}O$ (VSMOW) values (from ~+18–26‰ to ~+25–31‰) occurred between ca. 45 to 42 Ma (Fig. 6). Mulch et al. (2015) suggested that a portion of the upward increase in $\delta^{18}O$ values was due to development of a persistently stratified lacustrine setting and increasing evaporative enrichment of $\delta^{18}O$ and $\delta^{13}C$. Deposition of these strata also occurred during gradual global cooling (Pearson et al., 2001; Zachos et al., 2001), which might have served to decrease values of $\delta^{18}O$. If any portion of the increasing $\delta^{18}O$ values was related to topographic change, the data would suggest a local decrease in elevation during formation of the Elko Basin, preceding the arrival of local volcanism. However, this is speculative and geologic relations suggest that faulting was limited and that gradual sediment accumulation took place across northeast Nevada during this time (Henry et al., 2011).

By far the most significant change in $\delta^{18}O$ values observed in Fig. 6 is a ~12‰ decrease that occurred in late Eocene and/or Oligocene time. This decrease was first observed by Horton et al. (2004). They and others showed that similar, rapid decreases in $\delta^{18}O$ values occurred in carbonates throughout the North American Cordillera, following a south-younging pattern: A decrease from ~+20‰ to ~+13‰ between ca. 49–47 Ma in southwest Montana and eastern Idaho (Kent-Corson et al., 2006), followed by a decrease from ~+29‰ to ~+15‰ in the Elko Basin originally thought to have occurred between ca. 40.2–39.4 Ma (Mulch et al., 2015) but later revised to ca. 40–15.5 Ma by Lund Snee et al. (2016), and finally a ~4‰ decrease after ca. 23 Ma in southern Nevada (Chamberlain et al., 2012). This study more tightly constrains the magnitude and timing of the shift in the Elko Basin to a ~12‰ decrease in $\delta^{18}O$ values (~+27–+15‰) that likely initiated ca. 42 Ma, may have largely occurred by ca. 38.5 Ma, and was clearly complete by ca. 24 Ma (Fig. 6). This timing is corroborated by comparable negative isotopic

shifts ca. 44–40 Ma near this latitude in foreland basin deposits east of the Sevier fold and thrust belt (Fig. 1), which may have been related to drainages developed to the west and north that filled these basins (Carroll et al., 2008; Davis et al., 2009). The trend of south-younging decreases in $\delta^{18}O$ values has been interpreted to indicate south-migrating topographic uplift that coincided with intense, south-migrating volcanism (Horton et al., 2004; Mix et al., 2011; Chamberlain et al., 2012), supporting an early model by Gans (1990) based on geologic evidence.

In the Elko Basin, the large-magnitude negative isotopic shift shown in Fig. 6 appears to have initiated shortly before arrival of the first locally-erupted lavas and tuffs near the sampled sections (Figs. 2 and 3) ca. 39–38 Ma (Ressel and Henry, 2006; Henry et al., 2015; Lund Snee et al., 2016). The sign and magnitude of the decrease in $\delta^{18}O$ values is clearly consistent with an elevation increase in this region. It is inconsistent with models that require elevations to have decreased significantly at any point between ca. 42–10 Ma (e.g., Coney and Harms, 1984; Sonder et al., 1987; Bahadori et al., 2018; Cassel et al., 2018) because $\delta^{18}O$ values remain low throughout that interval (Fig. 6). We also note that the initiation of the negative $\delta^{18}O$ shift in the Elko Basin could reflect input of water (and sediment) from higher-elevation areas that might have developed further north shortly before this time (as the arrival of magmatism occurred earlier to the north, e.g., Konstantinou and Miller, 2015). In summary, it is unclear what proportion of this shift in northeast Nevada was due to elevation changes because it may have also coincided with changes in depositional setting, regional climate, and precipitation sources for drainages that fed this basin (Chamberlain et al., 2012; Mulch et al., 2015; Smith et al., 2017). Considering the present-day isotopic lapse rate of ~–1.5‰/km in the BRP (Lechler and Niemi, 2011a), clearly not all of the 12‰ decrease in $\delta^{18}O$ values could have been due to surface uplift, and much of it would therefore have been related to climate and/or diagenesis.

It is of course also possible that just the opposite—decreasing elevations—could have occurred at this time, with such a signal somehow obscured by climatic or diagenetic effects that caused the large magnitude decrease in $\delta^{18}O$ values. This appears unlikely for several reasons. The large-magnitude decrease in $\delta^{18}O$ values at this time is not reflected in the global climate record, which shows only gradual cooling (and generally increasing benthic $\delta^{18}O$ values) specifically in late Eocene time and more generally between 42–24 Ma (Zachos et al., 2001). Chamberlain et al. (2012) and Feng et al. (2013) noted that decreases in $\delta^{18}O$ values due to global cooling and

regional aridification in late Eocene and Oligocene time would have been dwarfed by isotopic changes due to topographic uplift. Focusing on the Elko Basin, Mulch et al. (2015) further considered the effects of climate and diagenesis, arguing that the pronounced decrease in $\delta^{18}O$ values in the basin during Eocene time (Fig. 6) could have been partly due to freshening of the lacustrine system due to warming during the Middle Eocene Climatic Optimum (MECO), combined with the onset of surface uplift. Based on our revised age assignments and the addition of age uncertainties into this discussion, it is clear from Fig. 6 that the measured isotopic data do not show short-wavelength changes that might indicate local effects of global climatic events. This suggests that the negative shift shown in Fig. 6 likely represents a more profound change—either climatic factors, diagenesis, and/or topography—that specifically affected this part of the Cordillera at approximately the time when voluminous volcanic activity began. That similar changes in isotopic values tracked volcanism southward through the North American Cordillera strongly suggests the onset of magmatism may have been an important influence on topography. The subsequent persistence of relatively low $\delta^{18}O$ values following the negative shift in the Elko Basin (Fig. 6) and throughout the North American Cordillera (Chamberlain et al., 2012) further indicates that the negative shift is likely not associated with transient changes in climate. Therefore, we agree with prior work indicating that a portion of this decrease in $\delta^{18}O$ values must have been related to topographic uplift.Subsequent to the large-magnitude decrease in $\delta^{18}O$ values, values of $\delta^{18}O$ and $\delta^{13}C$ remained generally low (but somewhat variable) throughout the sampled portion of the Humboldt Formation between ca. 24–12 Ma or later. However, $^{87}Sr/^{86}Sr$ increased dramatically within the middle part of the Humboldt Formation ca. 16–14 Ma (Mulch et al., 2015), which could reflect the first arrival of detritus supplied by the newly exposed adjacent Ruby Mountains–East Humboldt Range (REH) metamorphic core complex (MCC) (Figs. 1, 2, and 3), a result of Miocene fault uplift of the metamorphic and igneous rocks of the complex (Colgan et al., 2010; Lund Snee et al., 2016). Finally, the <5‰ increase in $\delta^{18}O$ values upward into the (approximately) middle Pliocene–middle Pleistocene Hay Ranch Formation (Horton et al., 2004) probably reflects a global rise of $\delta^{18}O$ values (Chamberlain et al., 2014), although it is also consistent with decreasing elevations of northern Nevada relative to central Nevada that occurred after middle or late Miocene time (Wallace et al., 2008; Camilleri et al., 2017).

5.2 Re-evaluating the evolution of the pre-Basin and Range drainage system

Rocks preserved within a network of mapped middle Cenozoic paleovalleys (Fig. 2) provide valuable insights for the region's topographic evolution independent from—but consistent with—the stable isotope record. Most of the dated rocks filling the paleovalleys are middle Cenozoic ignimbrites that flowed hundreds of km east and west along these channels, leaving deposits that have been linked to source calderas in Nevada (Henry, 2008). As calderas erupted, covering large parts of Nevada with ignimbrites, the flows traveled down paleochannels, away from a proposed paleodivide (Fig. 2), and progressively filled them (Henry and John, 2013).

We alternatively propose that the paleovalleys developed in response to localized topographic uplift during a time when significant magmatic material was added to the crust, with associated thermally driven uplift. Figure 2 shows the Cenozoic temporal evolution of volcanism together with the ages of oldest material dated within each paleodrainage (compiled from MacGinitie, 1941; Yeend, 1974; Goldstrand, 1992, 1994; Garside et al., 2005; Henry, 2008; Henry et al., 2012; Henry and John, 2013; Dumitru et al., 2015, 2016). The age of oldest dated material in each paleovalley decreases systematically southward, broadly accompanied by the southward progression of volcanism, suggesting that each drainage developed around the time that volcanism reached that particular latitude. Figure 7 presents a schematic snapshot of the proposed paleotopographic evolution ca. 36 Ma. We suggest that a highlands developed near the main eruptive centers at any given time and that the ~N–S-trending middle Cenozoic paleodivide proposed by Henry (2008), Henry et al. (2012), and Best et al. (2013) was a dynamic one, with the highest topography located above the region of the most active nested caldera centers.

Evolving southward-moving topography would have tended to disrupt pre-existing topography and drainages that were holdovers from the Late Cretaceous. Prior to volcanism, drainages likely flowed east and west away from the axis of the Cretaceous arc (Van Buer et al., 2009; Sharman et al., 2015). As magmatism swept south across the Sevier hinterland in Eocene and Oligocene time, creating its own topography, the divide would have shifted eastward to the main volcanic centers in central Nevada. Preexisting river channels might have been destroyed by uplift as magmatism migrated southward, including any south-flowing channels that formed on the southern ramp of the highlands at any given time (Fig. 7). The migrating volcanic front would have progressively filled any newly developed valleys with resistant volcanic rocks that eventually (because they blanketed the landscape) left behind an elevated, relatively flat plateau

such as described by Best et al. (2009), with surface elevations substantially altered by magmatic and thermal input into the crust.

Because the mapped paleochannels contain basal sedimentary deposits (Fig. S3) whose MDAs are only known in a handful of places (e.g., Henry, 2008), some paleovalleys could, of course, have developed before their oldest dated fill. Perhaps partly for this reason, it was previously assumed that this southward progression of oldest drainage fill occurred without any significant change in topography or drainage networks as volcanism migrated, and that the paleovalleys had existed since the Late Cretaceous (Henry, 2008; Best et al., 2009; Henry et al., 2012; Henry and John, 2013; Cassel et al., 2014, 2018). We note, however that it is unusual that there are no basal deposits in the mapped paleovalleys that have known ages significantly older than nearby magmatism. This is especially remarkable considering that ignimbrites were capable of traveling hundreds of km north and south of their eruptive centers (Henry and John, 2013). For each stage of migrating volcanism, earliest deposits are preserved near the source calderas, filling paleovalleys to the west, east, and sometimes north. Yet—critically—the record of fill preserved at the *bottoms* of paleovalleys (Fig. 2) shows few to no examples of eruptive products that would have had to travel significantly south (e.g., ≥100 km). The likeliest explanation is that most or all of these drainages simply did not exist significantly before magmatism began at a given latitude.

Thermally driven topographic uplift is an expected byproduct of both lithospheric thinning and addition of magmatic material (e.g., Lachenbruch and Morgan, 1990). Removal of the Farallon slab in middle Cenozoic time is thought to have caused asthenospheric upwelling and magmatism that would have thinned the lithosphere below the Great Basin (Humphreys, 1995). It is likely that these effects would have rapidly and dramatically increased elevations during the ignimbrite flareup. Analogous examples of uplift related to migrating volcanism and asthenospheric upwelling have been documented worldwide. Along the Yellowstone hotspot track (Snake River Plain on Fig. 1), east-migrating volcanism between middle Miocene time and the present was accompanied by pronounced uplift, faulting, and shifts of the continental divide (Anders and Sleep, 1992; Pierce et al., 1992; Coble and Mahood, 2016; Larimer et al., 2019). Uplift near Yellowstone, for example, has led to 1 km deep river incision since 3.6 Ma (Pierce and Morgan, 2009), which is comparable to the 1.2 km depth of the Great Basin paleovalleys (Henry et al., 2012). We propose that the same processes that are active today near Yellowstone

were active in the Great Basin, but at a grander scale, during the much more voluminous middle Cenozoic ignimbrite flareup magmatism.

5.3 Regional paleogeographic evolution

In this section, we present a summary view of the evolution of the Late Cretaceous to Cenozoic paleogeography of the northern Great Basin that we consider most likely given new and existing data and the geologic history of this region. This summary makes use of two critical interpretations described above: 1.) A pronounced decrease in $\delta^{18}O$ values in Cenozoic strata of northeast Nevada that might indicate substantial uplift approximately synchronous with arrival of Eocene volcanism, consistent with previous interpretations at other latitudes in the North American Cordillera, and 2.) That a south-younging pattern of material preserved at the bottom of middle Cenozoic paleodrainages suggests that drainage networks were reorganized synchronous with migrating volcanism. The timeline summarized below applies primarily to northeast Nevada where our study was conducted (right-hand panels of Fig. 6), but it is broadly applicable to the Sevier hinterland region of the northern Great Basin, especially where pertaining to regional tectonic events (left-hand panels of Fig. 6).

5.3.1 Late Cretaceous to middle Eocene (until ca. 46 Ma): Gradual erosion

For much of the early Cenozoic, northeast Nevada and much of the Sevier hinterland region experienced only modest erosion (Fig. 6) and limited surface expressions of tectonism. This inference is based on reconstructions of the middle Cenozoic unconformity, the development of paleogeologic maps representing the time before Basin and Range extension, and observation of generally low conodont alteration index values across much of the Great Basin (Gans and Miller, 1983; Gans et al., 1990; Crafford and Harris, 2005; Long, 2012; Konstantinou et al., 2012). Moreover, little or no deposition occurred within the Elko Basin during this time (Smith et al., 1976; Fouch et al., 1979; Haynes, 2003; Lund Snee et al., 2016). The regional topographic divide is inferred to have been located along the axis of youngest magmatism within the Mesozoic Sierra Nevada arc (Figs. 2 and 8a), as indicated by significantly higher magnitudes of erosion (~5–7 km) compared to 1–3 km across the back-arc region west of the Sevier fold and thrust belt (Van Buer et al., 2009). The signatures of detrital zircons from Late Cretaceous–Eocene sediments deposited in the California forearc also indicate derivation

623 from the Sierra Nevada magmatic arc (Figs. 1 and 2) and apparently not from further east
624 (Sharman et al., 2015) supporting the inference that the continental divide lay along the axis of
625 the Cretaceous arc at this time. Surface-cutting thrust faults were active along the Sevier belt in
626 the Late Cretaceous and they created topography as the thrust belt developed and shed its
627 erosional debris into the foreland basin. This is reflected both in the debris and in the Tertiary
628 unconformity map (e.g., Armstrong, 1968, 1972; Long, 2012; Konstantinou et al., 2012). The
629 Sevier thrust faults ceased most of their motion by Cenozoic time as deformation moved east to
630 the Rocky Mountains during the late Campanian to Eocene Laramide orogeny (e.g., DeCelles,
631 2004). This switch is linked to the onset of shallow slab subduction of the Farallon plate as
632 documented by both the cessation of magmatism in the Sierra Nevada arc and the eastward shift
633 in deformation (e.g., Dickinson and Snyder, 1978).
634 Surface-breaking faulting was limited and localized across the region of the Great Basin
635 in Late Cretaceous and Paleocene time (e.g., Burchfiel et al., 1992). The most significant
636 exception is the up to 3 km of normal slip on the high-angle Ninemile fault bounding the Sheep
637 Pass Basin (Druschke et al., 2009b) (Fig. 1). Localized deposition of conglomerate, siltstone, and
638 limestone in the Elko Basin before ca. 46 Ma (Lund Snee et al., 2016) could indicate modest
639 offset along normal faults that have not been clearly identified. These early deposits in the Elko
640 Basin, as well as the overlying Eocene Elko Formation, the Paleogene strata exposed in the
641 Sheep Pass Basin, and pre-volcanic conglomerate in the Sacramento Pass region of the Snake
642 Range (Fig. 1), contain clast compositions and detrital zircon age distributions that reflect
643 sediment recycling from strata mapped beneath the Cenozoic unconformity (Druschke et al.,
644 2011; Ruksznis, 2015; Lund Snee et al., 2016; Canada et al., 2020). All of these datasets appear
645 to preclude significant activity and offset along Late Cretaceous to Eocene faults across northeast
646 Nevada and, in general, the northern Great Basin. It has been the suggested that the evidence for
647 large-offset extensional faults at this time has been selectively obscured by Neogene faulting and
648 sediment deposition (Wells and Hoisch, 2012; Canada et al., 2020). We consider this view
649 unlikely because the reconstructions of strata beneath the Cenozoic unconformity, the Paleogene
650 detrital zircon record, and the evidence for minor pre-Miocene tilting all suggest limited pre-
651 Miocene faulting.
652

5.3.2 Middle Eocene (ca. 46–38 Ma): Shallow basins and early volcanism in northeast Nevada

A network of shallow basins (Fig. 2) developed in northeast Nevada in middle Eocene time (Fig. 6), by ca. 46 Ma and perhaps locally as early as ca. 49 Ma, as indicated by deposition of tuffs of these ages that likely arrived as air fall from eruptions in the Challis volcanic field in central Idaho (Haynes, 2003; Lund Snee et al., 2016; Smith et al., 2017). At about this time, the Farallon shallow slab is inferred to have begun to steepen (Fig. 8b), triggering upwelling of hot asthenosphere that contributed to an influx of massive volumes of magma and heat into the crust (e.g., Armstrong and Ward, 1991; Humphreys, 1995; Konstantinou et al., 2012; Konstantinou and Miller, 2015). Initiation of these basins may have slightly preceded the arrival of volcanism in northeast Nevada (Fig. 2) ca. 45–42 Ma (Brooks et al., 1995; Henry, 2008; Konstantinou et al., 2012). The timing of basin development and possible faulting in northeast Nevada suggests that these events were related to the onset of large-volume magmatism. Faulting shortly before, and in rare cases during, middle Cenozoic volcanism is also observed in numerous areas further to the south (Gans et al., 1989; Best and Christiansen, 1991; Druschke et al., 2009a; Ruksznis, 2015), perhaps as a result of the rapid but differential emplacement of voluminous magma bodies and heat transfer to the upper crust and/or localized thermal weakening of crust experiencing far field extensional strain.

It is noteworthy that (initiation of) the large-magnitude decrease in $\delta^{13}C$ and $\delta^{18}O$ values occurred immediately before arrival of volcanism to this specific region (Fig. 6) ca. 39–38 Ma (Ressel and Henry, 2006). The isotopic shifts were also approximately synchronous with a marked increase of heat input to the crust as indicated by increased high-T mineral (zircon and monazite) growth ca. 42 Ma at deeper levels of the crust now exposed in the REH MCC (Fig. 6) (Howard et al., 2011). Changes in surface elevation beginning about this time are also suggested by the first preserved volcanic fill in east- and west-flowing paleodrainages ca. 42–40 Ma (Fig. 2). As discussed above, our preferred hypothesis is that the mapped paleodrainages developed during magmatism, fundamentally changing an earlier landscape and replacing pre-existing drainage networks. The northern Elko Basin and the Copper Basin further north (Fig. 2) provide the first indications of an eastward shift of the topographic divide (Fig. 8b) in middle Eocene time as deposits preserved in some of these paleovalleys indicate both eastward and westward

flow of ignimbrites away from an area west and north of the Elko Basin (Fig. 2) in northern Nevada (Henry, 2018).

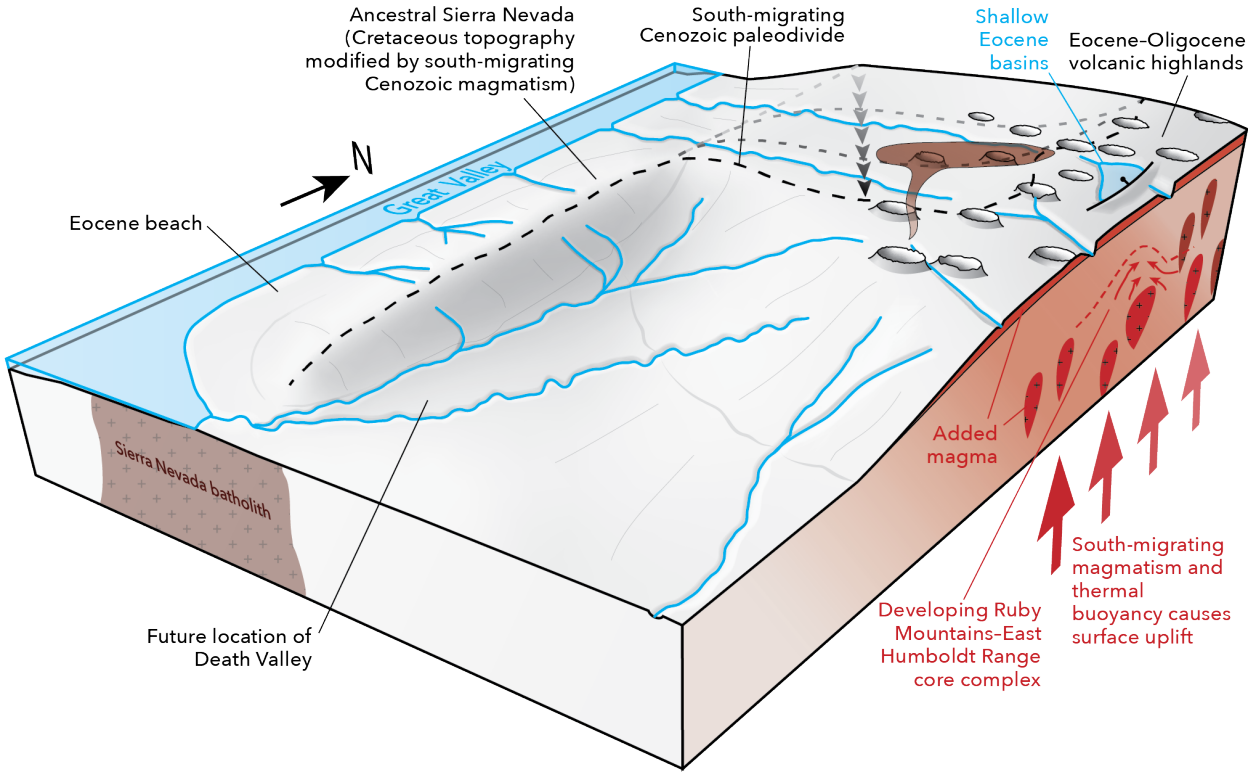

Figure 7. Schematic illustration of southward-migrating topographic uplift in the Great Basin related to the ignimbrite flare-up. This figure depicts a late Eocene (ca. 36 Ma) snapshot of thermally and magmatically supported volcanic highlands (to the north). At the latitude of the highlands, the drainage divide has shifted east from its Late Cretaceous to Paleocene position along the axis of the ancestral Sierra Nevada range (Van Buer et al., 2009) toward the center of the highlands. However, at latitudes further south, which have not yet experienced surface uplift, the divide remains along the ancestral Sierra Nevada range. Drainage networks have been reorganized near and north of the uplifted region, which remains elevated due to input of substantial heat (as indicated by ongoing partial melting in the Ruby Mountains–East Humboldt Range metamorphic core complex; Fig. 6) and voluminous volcanic and plutonic material to the crust.

5.3.3 Late Eocene (ca. 38–36 Ma): Active magmatism with volcanism

Sedimentation effectively ceased upon arrival of locally erupted volcanic rocks, which blanketed the study area with volcanic flows and ignimbrites beginning ca. 38 Ma (Haynes, 2003; Ressel and Henry, 2006; Lund Snee et al., 2016). These deposits left behind a vast, broadly flat regional volcanic tableland (Best et al., 2009) that persisted with little erosion until the onset

of Neogene Basin and Range faulting. This is documented by the widespread preservation of volcanic rocks above the Cenozoic unconformity across the entire northern Great Basin and adjacent Mesozoic Sierra batholith (e.g., Van Buer et al., 2009; Long, 2012; Konstantinou et al., 2012). Following the last eruption within the study area ca. 36.8 Ma (Lund Snee et al., 2016), magmatism continued to propagate southward (e.g., Ryskamp et al., 2008), likely in tandem with elevation gain (Gans, 1990).

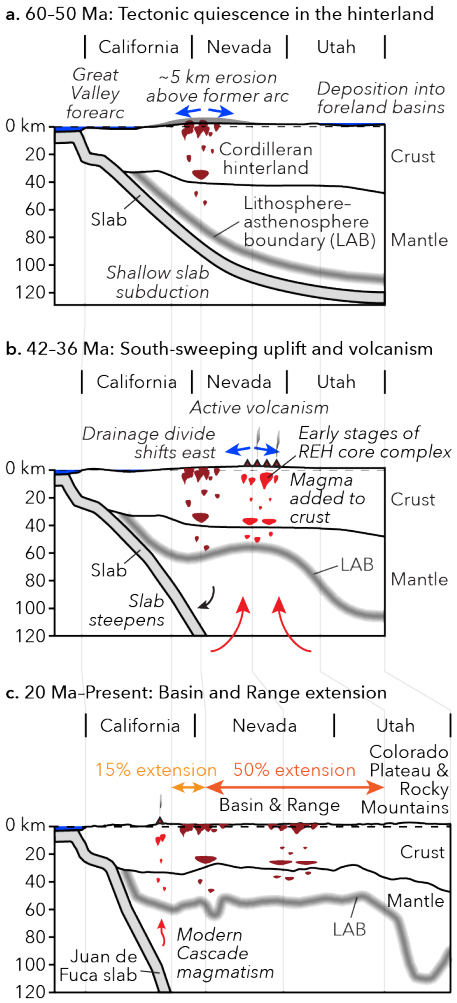

Figure 8. Cross sections along 40.5ºN latitude (line of section shown in Fig. 1) representing the lithospheric and topographic evolution of the northern Basin and Range province from Late Cretaceous time to the present. Present-day crustal thickness is from Shen and Ritzwoller (2016), the lithosphere–asthenosphere boundary is after the combined Sp–Ps interpretation of Levander and Miller (2012), and the Juan de Fuca slab position is after Tian and Zhao (2012) and McCrory et al. (2012).

5.3.4 Late Eocene to latest Oligocene (ca. 36–25.1 Ma): Volcanic quiescence with little erosion or faulting (but ongoing magmatism at depth)

It is well documented that partial melting and decompression continued in the deeper crust within the developing REH MCC and the Albion–Raft River–Grouse Creek (ARG) MCC to the north (Figs. 1 and 2) long after the cessation of surface volcanism (McGrew and Snee, 1994; McGrew et al., 2000; Howard et al., 2011; Konstantinou et al., 2013a; Lund Snee et al., 2016). The persistence of elevated temperatures, together with ongoing and prior magmatic additions to the crust, likely ensured continuing elevated topography. Remarkably, little surface deformation accompanied both magmatism and crustal flow at depth, except perhaps immediately above the MCCs, where the record is incomplete due to Neogene faulting and erosion (Colgan et al., 2010; Konstantinou et al., 2013a). Lund Snee et al. (2016) documented 10–15º tilting events between ca. 36.8–33.9 Ma and between ca. 31.1–24.4 Ma (now constrained between ca. 31.1–25.1 Ma) that they interpreted to represent local deformation associated with deeper crustal flow leading to surface adjustments in topography, either by faulting and/or doming in the developing MCC. A similar lack of significant surface deformation at this time is observed elsewhere across the region, including near the other Great Basin MCCs (Miller et al., 1999; Henry et al., 2011; Konstantinou et al., 2012; Ruksznis, 2015). The near absence of sedimentary deposits that span ca. 38–25 Ma (or later) in the study area (Fig. 6) and throughout the northern Great Basin (Henry et al., 2011) provides additional evidence that very little surface-breaking faulting occurred for at least 10 Ma following volcanism. This also suggests that the region did not experience significant subsidence, which might have created accommodation space for sediment deposition.

5.3.5 Latest Oligocene to middle Miocene (ca. 25.1–16.5 Ma): Little erosion and limited faulting

It is generally accepted that Basin and Range normal faulting and exhumation initiated ca. 17 Ma (e.g., Stockli, 2005; Colgan et al., 2010). However, the sedimentary record in the study area indicates that lacustrine sedimentation (an indication of the formation of accommodation space for sediment) was possibly associated with initial slip along Basin and Range faults as early as ca. 25.1 Ma, based on the MDA of the earliest lacustrine sediments deposited above Eocene and Oligocene volcanic rocks in the study area (Figs. 4b and 5). Minor deposition in the

latest Oligocene or earliest Miocene has also been recorded near the ARG and Snake Range MCCs (Gans et al., 1989; Miller et al., 1999; Konstantinou et al., 2012; Ruksznis, 2015).

5.3.6 Middle Miocene (ca. 16.5 Ma) to present: Rapid and then more gradual extension

Rapid slip along Basin and Range normal faults initiated ca. 17–16 Ma across most of the central part of the northern BRP (Figs. 1, 2, and 8c) and then propagated west, east, and north (Noble, 1972; Lund et al., 1993; Miller et al., 1999; Surpless et al., 2002; Stockli, 2005; Colgan et al., 2006, 2010; Lerch et al., 2008). Across this same region, the rate of extension decreased beginning ca. 12–10 Ma (e.g., Colgan and Henry, 2009) and continues at a slow rate today as active slip is primarily focused on faults now bounding the province (Thatcher et al., 1999; Kreemer et al., 2010). Measured $\delta^{18}O$ values were relatively low (mostly ≤15‰) before and during rapid fault slip and extension in the Elko Basin region, potentially implying that extension began across a region where elevations were already high.

Although the ~4‰ increase in $\delta^{18}O$ values that occurred in the study area before the middle Pliocene may not indicate elevation loss (as noted above), evidence from drainage patterns show that northern Nevada decreased in elevation relative to central Nevada after middle or late Miocene time (Wallace et al., 2008; Camilleri et al., 2017). In several other areas across Nevada and eastern California, a modest increase in $\delta^{18}O$ values (~2–5‰) occurred broadly between middle Miocene and late Pliocene time (in some cases perhaps beginning as early as early Miocene and elsewhere beginning as late as late Miocene), approximately at the same time as in the Elko region or perhaps slightly earlier (Poage and Chamberlain, 2002; Horton and Chamberlain, 2006; Kent-Corson et al., 2006). These suggestions are consistent with leaf physiognomic data from western Nevada, which suggest that elevations fell from ≤3 km around 16–15 Ma to <2 km by 14–12 Ma (Wolfe et al., 1997).

5.4 Implications for paleotopography including the *Nevadaplano* model

The paleogeographic and crustal evolution suggested by the synthesis of existing data with new data and improved age constraints that is presented here (Fig. 6) has direct implications for the topographic evolution of the region that lay between the axis of the Cretaceous arc and the Sevier thrust belt, often referred to as the "hinterland." A number of models for the Late Cretaceous and Cenozoic evolution of the hinterland across the Great Basin, especially those that

779 invoke a high plateau or *Nevadaplano* resulting from Mesozoic shortening, do not appear to be
780 compatible with geologic, geochronologic and isotope data as they bear on topography, faulting
781 and the evolution of drainage patterns. The *Nevadaplano* was originally defined by DeCelles
782 (2004) as a low-relief, high-elevation (potentially >3 km) plateau in eastern Nevada and western
783 Utah that was situated west of the Sevier fold and thrust belt and east of the Sierra Nevada (Fig.
784 1) in Late Cretaceous time (possibly forming as early as the Late Jurassic and persisting into the
785 Cenozoic).
786 Multiple lines of evidence presented here suggest that the region became a plateau-like
787 highlands much later than Mesozoic time, roughly synchronous with and continuing after
788 Cenozoic volcanism swept across the region (Fig. 2), before falling modestly to its present ~1.75
789 km elevations during and/or after Basin and Range extension. This growing database is also
790 inconsistent with suggestions that such a high plateau was supported by gravitationally unstable
791 crust overthickened by Mesozoic shortening (e.g., Sonder et al., 1987; Chase et al., 1998;
792 Druschke et al., 2009b; Wells et al., 2012; Wells and Hoisch, 2012) because of the lack of
793 evidence for significant extensional faulting until after the onset of Cenozoic magmatism.
794 Simply put, the heat budget represented by Cenozoic magmatism far exceeds that related to
795 thermal equilibration of crust thickened by thrust faulting. However, it is indeed likely that
796 topographic relief was low across most of the Sevier hinterland before middle Cenozoic time,
797 based on the depositional patterns of far-traveled Cenozoic ash-flow tuffs (Best et al., 2009) and
798 the modest magnitudes of pre-Eocene erosion and tilting documented in the Elko region (Brooks
799 et al., 1995; Henry et al., 2011; Lund Snee et al., 2016; Canada et al., 2019; this study) and
800 across the hinterland in general (Gans and Miller, 1983; Gans et al., 1990; Crafford and Harris,
801 2005; Van Buer et al., 2009; Long, 2012; Konstantinou et al., 2013b). Suggestions that the
802 hinterland was characterized by rugged, mountainous topography (Druschke et al., 2011; Snell et
803 al., 2014; Bahadori et al., 2018; Bahadori and Holt, 2019) are clearly at odds with these
804 observations.
805 Few constraints are available for absolute elevations of the Sevier hinterland during Late
806 Cretaceous and Cenozoic time. Snell et al. (2014) estimated ≥2 km elevation and potentially up
807 to 3.1 km in latest Cretaceous time in east-central Nevada by comparing measurements from
808 clumped isotope thermometry from lacustrine carbonates in the Sheep Pass Basin (Fig. 1) to
809 those in carbonates preserved within redbeds deposited near sea level in central Utah. This

measurement remains one of the only estimates for the time span before the onset of middle Cenozoic volcanism and its associated surface uplift. Measurements from Eocene fossil leaves in Copper Basin (Figs. 1 and 2), representing the time approximately at the onset of volcanism, provide widely distributed elevation estimates ranging from 0.6–1.2 km (Christiansen and Yeats, 1992) and 1.6 ± 1.6 km (Chase et al., 1998), to 2.0 ± 0.2 km (Wolfe et al., 1998) and 2.8 ± 1.8 km (Chase et al., 1998). This broad range complicates efforts to employ these estimates quantitatively. We consider estimates that some paleovalleys reached up to 1.2 km deep, and in some cases possibly more (Henry et al., 2012), to provide the most definite minimum bounds on hinterland elevation. However, those estimates only reflect the time when the paleovalleys were active, which we suggest was likely upon the arrival of magmatic activity that varied by latitude between middle Eocene and middle Miocene time (Figs. 2 and 7).

Other studies focused on the volcanic rocks erupted across the Great Basin (including the Elko region) and westward to the Sierra Nevada flank have argued that a high plateau persisted across the former Sevier hinterland between 41–23 Ma on the basis of relatively low δD values in altered volcanic glass (Cassel et al., 2009, 2014, 2018). However, the δD values vary considerably over time and space. This led Cassel et al. (2018) to propose that elevations across the hinterland were ~2.25–3.0 km in late Eocene time and then fell by ~0.5–1 km by early Oligocene time, followed by ~1.5 km uplift between the early and late Oligocene to as high as 3.5 km in central Nevada, before eventually falling to present-day mean elevations around 1.75 km. Such oscillatory elevation changes are not compatible with the contemporaneous δ^{18}O record of the Elko Basin region (Fig. 6). They are also difficult to reconcile with geologic evidence as they would seem to imply multiple episodes of substantial faulting and sedimentation. The volcanic glass δD measurements were obtained from a wide range of latitudes across the Great Basin and surroundings, under the assumption that elevations at any time period would be comparable at different locations (see Cassel et al., 2018). If elevations were strongly affected by migrating magmatism, as we suggest, then this assumption is invalid.

It is possible that the middle Cenozoic uplift that we document here simply added to already high elevations (≥2 km) that were the result of crustal thickening during Sevier fold and thrust belt development. There are several reasons why this is unlikely. First, further elevation increase above already high values would require later high-magnitude elevation loss through erosion or extensional collapse that is not clearly demonstrated in the geologic or isotopic

841 records. Second, marine fossils, stable isotope data, and detrital populations show that the
842 southern Sierra Nevada and areas slightly to the east (~35.5ºN latitude), which have a similar
843 geologic history to the Great Basin, were *at or near sea level* in the Paleocene and remained very
844 low (<1 km) into Eocene time (Lofgren et al., 2008; Lechler and Niemi, 2011b). Eocene time is
845 exactly when a high plateau associated with crustal thickening should have been present in that
846 region. If a significantly elevated plateau was present across the Great Basin in Late Cretaceous
847 and Paleogene time, then it would have been limited to areas north of ~37–38ºN and bounded on
848 the south by a steep ramp leading nearly to sea level. Third, the apparent absence of detritus
849 sourced from the Sevier hinterland in Late Cretaceous to early Eocene sediments of the northern
850 California forearc (Sharman et al., 2015) suggests that river systems in Nevada may not have
851 flowed west across the Sierra Nevada batholith (as suggested by Cassel et al., 2012b) or north
852 into the Late Cretaceous Kione (Dumitru et al., 2016) or early Eocene Princeton (Dumitru et al.,
853 2012) paleorivers during this time. The first U-Pb detrital zircon age population that could
854 represent deposition into the northern California forearc from northeastern Nevada has been
855 detected in deposits of the middle Eocene Upper Markley Formation sandstone near San
856 Francisco Bay (Gooley et al., in review). This suggests that, from Late Cretaceous through early
857 Eocene time, much of Nevada was lower than the area of the Mesozoic Sierra Nevada batholith
858 to the west (Fig. 1) and also not able to drain northward into Idaho and Oregon. Fourth and
859 finally, it is challenging to explain dramatic elevation losses such as those proposed by, e.g., Best
860 et al. (2009) given updated estimates of only moderate (40–50%) magnitudes of total extension
861 across the Great Basin (e.g., Colgan and Henry, 2009; Long, 2018).
862
863 **5.5 Implications for crustal thickness**
864 The data presented here are incompatible with suggestions that crustal thicknesses
865 became so great during Mesozoic shortening that they led to gravitationally driven extensional
866 collapse (e.g., Wells et al., 2012), for at least two reasons. First, the stable isotope and geologic
867 data suggest a pronounced elevation increase, not decrease, in middle Cenozoic time, long after
868 Mesozoic shortening. After this, $\delta^{18}O$ remained low through middle Miocene time, suggesting
869 that elevations stayed approximately the same long after volcanism, which is consistent with the
870 inferred large volumes of magmatic material added to the crust and evidence that high crustal
871 temperatures were maintained up to the time when basin-and-range faulting began (Fig. 6).

Evidence for topographic gain rather than extensional collapse in Paleogene time implies that crustal thickness was probably not a primary cause of topographic changes. This evidence for regionally modest and relatively unchanging elevation followed by topographic gain in middle Cenozoic time also directly contradicts suggestions that elevations of the Colorado Plateau increased markedly in Late Mesozoic to Paleogene time due to channelized flow of ductile lower crust eastward from the hinterland toward the Colorado Plateau (e.g., McQuarrie and Chase, 2000).

Second, the timing and magnitude of extensional events are not compatible with collapse of overthickened crust. Not only did appreciable extension not take place until the middle Miocene (e.g., Colgan and Henry, 2009; Konstantinou and Miller, 2015), long after the end of shortening, but estimates for only 40–50% total extension across the northern BRP (McQuarrie and Wernicke, 2005; Colgan and Henry, 2009; Long, 2018) are insufficient (when restored) to yield crustal thicknesses of 60 km or more, as has been assumed by a number of studies invoking this model (e.g., Sonder et al., 1987; McQuarrie and Chase, 2000; DeCelles and Coogan, 2006; Best et al., 2009). Restoration of extension across the northern BRP at ~39ºN (Fig. 2) yielded a mean pre-extensional (but post-volcanic) crustal thickness of ~54 km, reaching up to ~60 km in a zone crossing the Nevada–Utah border that includes the Sevier Desert (Long, 2018) and coinciding with the ~N–S-trending crustal welt that developed due to thrusting in the Sevier belt. Accounting for potentially multiple km of magmatic addition to the crust in Cenozoic time could reduce this estimated mean to ~50 km. In fact, the ~50% extension estimate by McQuarrie and Wernicke (2005) and the ~46% estimate by Long (2018) are upper bounds because both assumed large magnitudes of low-angle normal slip on the controversial (e.g., Anders and Christie-Blick, 1994) Sevier Desert detachment. Assuming mass balance along strike and accounting for the present-day crustal thicknesses of ~31±3 km (e.g., Shen and Ritzwoller, 2016), the estimates of extension suggest instead that mean crustal thicknesses of ~45–50 km underpinned the region following shortening and might have been even less after considering Cenozoic magmatic addition.

A sophisticated 2D (map view) model by Bahadori et al. (2018), showed that retrodeforming crustal thicknesses based on the restoration by McQuarrie and Wernicke (2005), together with an isostatic compensation model, would produce a narrow, tall (crest ≥4 km and peaks >6 km) mountain range atop the narrow welt of crust ~55–60 km thick suggested by Long

(2018). Flanking the crustal welt, their model yielded very thin (~30–45 km) crust over most of central and western Nevada. The modeled mountain chain is significantly (≥200 km in northern and central Nevada) east of the middle Cenozoic paleodivide inferred by Henry et al. (2012) and Best et al. (2013) using the paleoflow directions of channelized ignimbrites, and incompatible with the broad, migrating highlands that we propose (Figs. 2 and 7). The suggestion of a rugged, ≥4 km-tall mountain belt along the Utah-Nevada border is also at odds with indications that pre-volcanic erosion magnitudes were modest and smoothly distributed throughout the area of the inferred crustal welt (Gans and Miller, 1983; Miller and Gans, 1989; Long, 2012; Konstantinou et al., 2012). The disagreement between the geologic data and the crustal thicknesses and topography estimates suggests the need for retrodeformation studies that consider the limited crustal thicknesses that lay beneath the passive margin sequence west of its depositional hingeline, use of updated models of Cenozoic extension, and greater focus on regional-scale lower crustal flow that would flatten the Moho during extension (Gans, 1987).

5 CONCLUSIONS

In this paper, we have added new stable isotope measurements, geochronology, and geologic mapping from the Elko Basin region of northeast Nevada to a large body of previously published data in order to clarify and place tighter temporal brackets on the geologic evolution of this region and the surrounding northern Great Basin throughout the Late Cretaceous to Miocene time interval. The data are in turn used to evaluate the multitude of hypotheses about the crustal thickness, crustal evolution, onset of extension, and topographic elevation and relief of the hinterland region between the Sierra Nevada Cretaceous arc and the Sevier foreland fold and thrust belt to the east (Fig. 1). Multiple lines of evidence discussed here suggest that the Sevier hinterland was a broad, low-relief plain subject to only modest erosion from the Late Cretaceous through much of Paleogene time. During that time, the continental divide lay along the axis of the Cretaceous arc. Minor-offset faulting, tilting and sedimentation began in the middle Eocene, likely contemporaneous with a major (~12‰) decrease in $\delta^{18}O$ values. The isotopic shift forms part of a regional trend of south-younging negative isotopic shifts documented in fluvial-lacustrine carbonates that, together with geologic data, suggest diachronous topographic uplift that approximately tracks surface volcanism (Gans, 1990; Kent-Corson et al., 2006; Mix et al., 2011; Chamberlain et al., 2012).

Due to appreciable magmatic inflation and thermally-driven uplift, the drainage divide located along the axis of the Cretaceous arc (Van Buer et al., 2009; Sharman et al., 2015) stepped eastward to northeast Nevada in a south-progressing fashion (Figs. 7 and 8). We envisage that migrating magmatism produced broad, southward-growing highlands, forming a divide centered on the areas of highest caldera density and thermal input into the crust (Fig. 8b). The highlands would have maintained much of their elevation long after being established, and up to the onset of basin and range faulting, due to the continued addition of magma and heat to the crust, the latter of which has been documented to have occurred at least to 25 Ma (McGrew and Snee, 1994; Strickland et al., 2011; Konstantinou et al., 2012, 2013a; Konstantinou and Miller, 2015). Uplift roughly coincident with onset of volcanism (Fig. 7) appears to be the simplest explanation for the south-younging pattern of oldest fill recorded in the network of mapped middle Cenozoic paleodrainages across much of the Great Basin (Fig. 2), suggesting that pre-existing drainages were profoundly disrupted and their deposits mostly eroded away as the highlands migrated southward.

Eventually, rapid Basin and Range extension between ca. 17–10 Ma (e.g., Stockli, 2005; Colgan, 2013) reduced the crust to its present ~30 km thickness (e.g., Shen and Ritzwoller, 2016), from peak thicknesses that reached averages of only ~45–50 km *after* addition of Cenozoic magmas. A later episode of drainage reorganization indicates that elevation in northern Nevada declined relative to central Nevada beginning after middle or late Miocene time (Wallace et al., 2008; Camilleri et al., 2017). It is notable that appreciable extension began long after Mesozoic shortening and middle Cenozoic volcanism . This timing, together with the evidence for migrating topography presented here, is incompatible with models that propose that extension was driven by gravitational collapse of a high plateau that developed due to Mesozoic crustal shortening. Instead, rapid extension in middle Miocene time was likely caused by a combination of removal of the flat-subducting Farallon slab (Armstrong and Ward, 1991) and changing tectonic boundary conditions associated with development of the San Andreas transform margin (see Spencer and Normark, 1979; Stock and Hodges, 1989; Dickinson, 2002; Colgan and Henry, 2009; Bahadori and Holt, 2019). These events allowed extension to occur rapidly along a vast region of thermally weakened crust beneath the future Basin and Range ca. 17 Ma (e.g., Stockli, 2005). Extension was likely driven by thermal elevation and gravitational potential energy that remained high following intense middle Cenozoic magmatism.

ACKNOWLEDGEMENTS

This research was funded by NSF grant EAR-1322084 to Miller and a Stanford University G.J. Lieberman Fellowship to Lund Snee. We thank Peter M. Blisniuk for running the stable isotope analyses, Trevor A. Dumitru for guidance with detrital zircon geochronology, M. Raftrey for analyzing four detrital zircon samples, and Stephen Pearcey and Virginia Isava for assisting with sampling. The manuscript benefitted from discussions with Simon L. Klemperer, George A. Thompson, Joseph P. Colgan, Karen I. Lund, and Norm H. Sleep. We are especially grateful to C. Page Chamberlain for sharing detailed knowledge about the regional isotopic record, providing comments on early versions of the manuscript, and allowing samples to be run at the Stanford Stable Isotope Biogeochemistry Laboratory. The authors declare no conflicts of interest. Data tables supporting the stable isotope analysis and geochronology are included in the Supplementary Information, together with detailed descriptions of analytical methods and techniques for establishing depositional age constraints.

REFERENCES

Anders, M.H., and Christie-Blick, N., 1994, Is the Sevier Desert reflection of west-central Utah a normal fault? Geology, v. 22, p. 771, doi:10.1130/0091-7613(1994)022<0771:ITSDRO>2.3.CO;2.

Anders, M.H., and Sleep, N.H., 1992, Magmatism and Extension - The Thermal and Mechanical Effects of the Yellowstone Hotspot: Journal of Geophysical Research, v. 97, p. 15,379-15,393, doi:10.1029/92JB01376.

Armstrong, R.L., 1970, Geochronology of Tertiary igneous rocks, eastern Basin and Range Province, western Utah, eastern Nevada, and vicinity, U.S.A.: Geochimica et Cosmochimica Acta, v. 34, p. 203–232, doi:10.1016/0016-7037(70)90007-4.

Armstrong, R.L., 1972, Low-angle (denudation) faults, hinterland of the sevier orogenic belt, eastern nevada and western utah: Bulletin of the Geological Society of America, v. 83, p. 1729–1754, doi:10.1130/0016-7606(1972)83[1729:LDFHOT]2.0.CO;2.

Armstrong, R.L., 1968, Sevier Orogenic Belt in Nevada and Utah: Geological Society of America Bulletin, v. 79, p. 429, doi:10.1130/0016-7606(1968)79[429:SOBINA]2.0.CO;2.

Armstrong, R.L., and Ward, P., 1991, Evolving geographic patterns of Cenozoic magmatism in the North American Cordillera: The temporal and spatial association of magmatism and metamorphic core complexes: Journal of Geophysical Research, v. 96, p. 13201, doi:10.1029/91JB00412.

Atwater, T., 1989, Plate tectonic history of the northeast Pacific and western North America, *in* Winterer, E.L., Hussong, D.M., and Decker, R.W. eds., The Geology of North America: The Eastern Pacific Ocean and Hawaii, v. N, p. 499–522.

1003 Bahadori, A., and Holt, W.E., 2019, Geodynamic evolution of southwestern North America since
1004 the Late Eocene: Nature Communications, v. 10, p. 1–18, doi:10.1038/s41467-019-12950-8.
1005 Bahadori, A., Holt, W.E., and Rasbury, E.T., 2018, Reconstruction modeling of crustal thickness
1006 and paleotopography of western North America since 36 Ma: Geosphere, v. 14, p. 1207–
1007 1231, doi:10.1130/GES01604.1.
1008 Best, M.G., Barr, D.L., Christiansen, E.H., Gromme, S., Deino, A.L., and Tingey, D.G., 2009,
1009 The Great Basin Altiplano during the middle Cenozoic ignimbrite flareup: insights from
1010 volcanic rocks: International Geology Review, v. 51, p. 589–633,
1011 doi:10.1080/00206810902867690.
1012 Best, M.G., and Christiansen, E.H., 1991, Limited extension during peak Tertiary volcanism,
1013 Great Basin of Nevada and Utah: Journal of Geophysical Research, v. 96, p. 13509,
1014 doi:10.1029/91JB00244.
1015 Best, M.G., Christiansen, E.H., and Gromme, S., 2013, Introduction: The 36-18 Ma southern
1016 Great Basin, USA, ignimbrite province and flareup: Swarms of subduction-related
1017 supervolcanoes: Geosphere, v. 9, p. 260–274, doi:10.1130/GES00870.1.
1018 Blisniuk, P.M., and Stern, L. a., 2005, Stable isotope paleoaltimetry: A critical review: American
1019 Journal of Science, v. 305, p. 1033–1074, doi:10.2475/ajs.305.10.1033.
1020 Du Bray, E. a., 2007, Time, space, and composition relations among northern Nevada intrusive
1021 rocks and their metallogenic implications: Geosphere, v. 3, p. 381–405,
1022 doi:10.1130/GES00109.1.
1023 Brooks, W.E., Thorman, C.H., Snee, L.W., and Al, B.E.T., 1995, Ar ages and tectonic setting of
1024 the middle Eocene northeast Nevada volcanic field: Journal of Geophysical Research, v.
1025 100, p. 10403, doi:10.1029/94JB03389.
1026 Van Buer, N.J., and Miller, E.L., 2010, Sahwave Batholith, NW Nevada: Cretaceous arc flare-up
1027 in a basinal terrane: Lithosphere, v. 2, p. 423–446, doi:10.1130/L105.1.
1028 Van Buer, N.J., Miller, E.L., and Dumitru, T.A., 2009, Early Tertiary paleogeologic map of the
1029 northern Sierra Nevada batholith and the northwestern Basin and Range: Geology, v. 37, p.
1030 371–374, doi:10.1130/G25448A.1.
1031 Burchfiel, C., Cowan, D.S., and Davis, G.A., 1992, Tectonic overview of the Cordilleran orogen
1032 in the western United States, *in* Burchfiel, B.C., Lipman, P.W., and Zoback, M.L. eds., The
1033 Geology of North America, v. G-3, p. 407–479.
1034 Camilleri, P.A., Deibert, J., and Perkins, M.E., 2017, Middle Miocene to Holocene tectonics,
1035 basin evolution, and paleogeography along the southern margin of the Snake River Plain in
1036 the Knoll Mountain-Ruby-East Humboldt Range region, northeastern Nevada and south-
1037 central Idaho: Geosphere, v. 13, p. 1901–1948, doi:10.1130/GES01318.1.
1038 Canada, A.S., Cassel, E.J., Stockli, D.F., Smith, M.E., Jicha, B.R., and Singer, B.S., 2020,
1039 Accelerating exhumation in the Eocene North American Cordilleran hinterland:
1040 Implications from detrital zircon (U-Th)/(He-Pb) double dating: GSA Bulletin, v. 132, p.
1041 198–214, doi:10.1130/B35160.1.
1042 Carroll, A.R., Doebbert, A.C., Booth, A.L., Chamberlain, C.P., Rhodes-Carson, M.K., Smith,
1043 M.E., Johnson, C.M., and Beard, B.L., 2008, Capture of high-altitude precipitation by a
1044 low-altitude Eocene lake, western U.S: Geology, v. 36, p. 791–794,
1045 doi:10.1130/G24783A.1.
1046 Cassel, E.J., Breecker, D.O., Henry, C.D., Larson, T.E., and Stockli, D.F., 2014, Profile of a
1047 paleo-orogen: High topography across the present-day Basin and Range from 40 to 23 Ma:
1048 Geology, v. 42, p. 1007–1010, doi:10.1130/G35924.1.

1049 Cassel, E.J., Graham, S.A., and Chamberlain, C.P., 2009, Cenozoic tectonic and topographic
1050 evolution of the northern Sierra Nevada, California, through stable isotope paleoaltimetry in
1051 volcanic glass: Geology, v. 37, p. 547–550, doi:10.1130/G25572A.1.
1052 Cassel, E.J., Graham, S.A., Chamberlain, C.P., and Henry, C.D., 2012a, Early Cenozoic
1053 topography, morphology, and tectonics of the northern Sierra Nevada and western Basin
1054 and Range: Geosphere, v. 8, p. 229–249, doi:10.1130/GES00671.1.
1055 Cassel, E.J., Grove, M., and Graham, S.A., 2012b, Eocene drainage evolution and erosion of the
1056 Sierra Nevada batholith across northern California and Nevada: American Journal of
1057 Science, v. 312, p. 117–144, doi:10.2475/02.2012.03.
1058 Cassel, E.J., Smith, M.E., and Jicha, B.R., 2018, The Impact of Slab Rollback on Earth's
1059 Surface: Uplift and Extension in the Hinterland of the North American Cordillera:
1060 Geophysical Research Letters, p. 1–9, doi:10.1029/2018GL079887.
1061 Catchings, R.D., and Mooney, W.D., 1991, Basin and range crustal and upper mantle structure,
1062 northwest to central Nevada: Journal of Geophysical Research, v. 96, p. 6247,
1063 doi:10.1029/91JB00194.
1064 Chamberlain, C.P., Mix, H.T., Mulch, A., Hren, M.T., Kent-Corson, M.L., Davis, S.J., Horton,
1065 T.W., and Graham, S.A., 2012, The Cenozoic climatic and topographic evolution of the
1066 western North American Cordillera: American Journal of Science, v. 312, p. 213–262,
1067 doi:10.2475/02.2012.05.
1068 Chamberlain, C.P., Mulch, A., Kent-Corson, M.L., Davis, S.J., Carroll, A.R., and Graham, S.A.,
1069 2007, Cenozoic topographic evolution of the Western North America Cordillera:
1070 Geochimica Et Cosmochimica Acta, v. 71, p. A157–A157.
1071 Chamberlain, C.P., Winnick, M.J., Mix, H.T., Chamberlain, S.D., and Maher, K., 2014, The
1072 impact of neogene grassland expansion and aridification on the isotopic composition of
1073 continental precipitation: Global Biogeochemical Cycles, v. 28, p. 992–1004,
1074 doi:10.1002/2014GB004822.
1075 Chase, C.G., Gregory-Wodzicki, K., Parrish, J.T., and DeCelles, P.G., 1998, Topographic history
1076 of the Western Cordillera of North America and controls on climate, *in* Crowley, T.J. and
1077 Burke, K. eds., Tectonic boundary conditions for climate reconstructions, Oxford
1078 University Press, v. 39, p. 73–99,
1079 https://books.google.ch/books?hl=en&lr=&id=HbamVUkDTLMC&oi=fnd&pg=PA73&dq
1080 =chase+1998+western+cordillera&ots=qen7llUxn_&sig=WUIfZKMs-
1081 fTiRgSKQKshUJ8wYUk#v=onepage&q=chase 1998 western cordillera&f=false.
1082 Christiansen, R.L., and Yeats, R.S., 1992, Post-Laramide geology of the US Cordilleran region,
1083 *in* Burchfiel, B.C., Lipman, P.W., and Zoback, M.L. eds., The Geology of North America,
1084 v. 3, p. 261–406.
1085 Coble, M.A., and Mahood, G.A., 2016, Geology of the High Rock caldera complex, northwest
1086 Nevada, and implications for intense rhyolitic volcanism associated with flood basalt
1087 magmatism and the initiation of the Snake River Plain- Yellowstone trend: Geosphere, v.
1088 12, p. 58–113, doi:10.1130/GES01162.1.
1089 Coble, M.A., and Mahood, G.A., 2012, Initial impingement of the Yellowstone plume located by
1090 widespread silicic volcanism contemporaneous with Columbia River flood basalts:
1091 Geology, v. 40, p. 655–658, doi:10.1130/G32692.1.
1092 Colgan, J.P., 2013, Reappraisal of the relationship between the northern Nevada rift and Miocene
1093 extension in the northern Basin and Range Province: Geology, v. 41, p. 211–214,
1094 doi:10.1130/G33512.1.

1095 Colgan, J.P., Dumitru, T.A., McWilliams, M.O., and Miller, E.L., 2006, Timing of Cenozoic
1096 volcanism and Basin and Range extension in northwestern Nevada: New constraints from
1097 the northern Pine Forest Range: Bulletin of the Geological Society of America, v. 118, p.
1098 126–139, doi:10.1130/B25681.1.
1099 Colgan, J.P., and Henry, C.D., 2009, Rapid middle Miocene collapse of the Mesozoic orogenic
1100 plateau in north-central Nevada: International Geology Review, v. 51, p. 920–961,
1101 doi:10.1080/00206810903056731.
1102 Colgan, J.P., Howard, K.A., Fleck, R.J., and Wooden, J.L.P., 2010, Rapid middle Miocene
1103 extension and unroofing of the southern Ruby Mountains, Nevada: Tectonics, v. 29, p. 417,
1104 doi:10.1029/2009TC002655.
1105 Coney, P.J., and Harms, T.A., 1984, Cordilleran metamorphic core complexes: Cenozoic
1106 extensional relics of Mesozoic compression: Geology, v. 12, p. 550–554, doi:10.1130/0091-
1107 7613(1984)12<550:CMCCCE>2.0.CO;2.
1108 Crafford, A.E.J., 2007, Geologic Map of Nevada: US Geological Survey Data Series 249: U.S.
1109 Geological Survey Data Series 249, p. 46.
1110 Crafford, A.E.J., and Harris, A.G., 2005, New digital conodont color alteration index (CAI)
1111 maps of Nevada, *in* Geological Society of America Abstracts with Programs, Salt Lake
1112 City, Utah, v. 37, p. 379,
1113 https://gsa.confex.com/gsa/2005AM/finalprogram/abstract_94308.htm.
1114 Davis, S.J., Mix, H.T., Wiegand, B.A., Carroll, A.R., and Chamberlain, C.P., 2009, Synorogenic
1115 evolution of large-scale drainage patterns: Isotope paleohydrology of sequential laramide
1116 basins: American Journal of Science, v. 309, p. 549–602, doi:10.2475/07.2009.02.
1117 DeCelles, P.G., 2004, Late Jurassic to Eocene evolution of the Cordilleran thrust belt and
1118 foreland basin system, western U.S.A.: American Journal of Science, v. 304, p. 105–168,
1119 doi:10.2475/ajs.304.2.105.
1120 DeCelles, P.G., and Coogan, J.C., 2006, Regional structure and kinematic history of the Sevier
1121 fold-and-thrust belt, central Utah: Bulletin of the Geological Society of America, v. 118, p.
1122 841–864, doi:10.1130/B25759.1.
1123 Dickinson, W.R., 2013, Phanerozoic palinspastic reconstructions of Great Basin geotectonics
1124 (Nevada-Utah, USA): Geosphere, v. 9, p. 1384–1396, doi:10.1130/GES00888.1.
1125 Dickinson, W.R., 2002, The Basin and Range Province as a Composite Extensional Domain:
1126 International Geology Review, v. 44, p. 1–38, doi:10.2747/0020-6814.44.1.1.
1127 Dickinson, W.R., and Snyder, W.S., 1978, Plate tectonics of the Laramide orogeny, *in*
1128 Geological Society of America Memoir, v. 151, p. 355–366, doi:10.1130/MEM151-p355.
1129 Druschke, P., Hanson, A.D., and Wells, M.L., 2009a, Structural, stratigraphic, and
1130 geochronologic evidence for extension predating Palaeogene volcanism in the Sevier
1131 hinterland, east-central Nevada: International Geology Review, v. 51, p. 743–775,
1132 doi:10.1080/00206810902917941.
1133 Druschke, P., Hanson, a. D., Wells, M.L., Gehrels, G.E., and Stockli, D.F., 2011,
1134 Paleogeographic isolation of the cretaceous to eocene sevier hinterland, east-central nevada:
1135 Insights from U-Pb and (U-Th)/he detrital zircon ages of hinterland strata: Bulletin of the
1136 Geological Society of America, v. 123, p. 1141–1160, doi:10.1130/B30029.1.
1137 Druschke, P., Hanson, A.D., Wells, M.L., Rasbury, T., Stockli, D.F., and Gehrels, G.E., 2009b,
1138 Synconvergent surface-breaking normal faults of Late Cretaceous age within the Sevier
1139 hinterland, east-central Nevada: Geology, v. 37, p. 447–450, doi:10.1130/G25546A.1.
1140 Dumitru, T.A., Elder, W.P., Hourigan, J.K., Chapman, A.D., Graham, S.A., and Wakabayashi,

J., 2016, Four Cordilleran paleorivers that connected Sevier thrust zones in Idaho to depocenters in California, Washington, Wyoming, and, indirectly, Alaska: Geology, v. 44, p. 75–78, doi:10.1130/G37286.1.
Dumitru, T.A., Ernst, W.G., Hourigan, J.K., and McLaughlin, R.J., 2015, Detrital zircon U–Pb reconnaissance of the Franciscan subduction complex in northwestern California: International Geology Review, v. 57, p. 767–800, doi:10.1080/00206814.2015.1008060.
Dumitru, T.A., Ernst, W.G., Wright, J.E., Wooden, J.L.P., Wells, R.E., Farmer, L.P., Kent, A.J.R., and Graham, S.A., 2012, Eocene extension in Idaho generated massive sediment floods into the Franciscan trench and into the Tyee, Great Valley, and Green River basins: Geology, v. 41, p. 187–190, doi:10.1130/G33746.1.
Ehlers, T.A., and Poulsen, C.J., 2009, Influence of Andean uplift on climate and paleoaltimetry estimates: Earth and Planetary Science Letters, v. 281, p. 238–248, doi:10.1016/j.epsl.2009.02.026.
Feng, R., Poulsen, C.J., Werner, M., Chamberlain, C.P., Mix, H.T., and Mulch, A., 2013, Early cenozoic evolution of topography, climate, and stable isotopes in precipitation in the north American cordillera: American Journal of Science, v. 313, p. 613–648, doi:10.2475/07.2013.01.
Fiorella, R.P., Poulsen, C.J., Pillco Zolá, R.S., Jeffery, M.L., and Ehlers, T.A., 2015, Modern and long-term evaporation of central Andes surface waters suggests paleo archives underestimate Neogene elevations: Earth and Planetary Science Letters, v. 432, p. 59–72, doi:10.1016/j.epsl.2015.09.045.
Fouch, T.D., Hanley, J.H., and Forester, R.M., 1979, Preliminary Correlation of Cretaceous and Paleogene lacustrine and related nonmarine sedimentary and volcanic rocks in parts of the eastern Great Basin of Nevada and Utah, *in* 1979 Basin and Range Symposium, Rocky Mountain Association of Geologists, v. 69, p. 305–312.
Gans, P.B., 1987, An open-system, two-layer crustal stretching model for the Eastern Great Basin: Tectonics, v. 6, p. 1–12, doi:10.1029/TC006i001p00001.
Gans, P.B., 1990, Space-time patterns of Cenozoic NS extension, NS shortening, EW extension, and magmatism in the Basin and Range Province: Evidence for active rifting, *in* Geological Society of America Abstracts with Programs, v. 22, p. 24.
Gans, P.B., Mahood, G.A., and Schermer, E., 1989, Synextensional magmatism in the Basin and Range Province; A case study from the eastern Great Basin: GSA Special Papers, v. 233, p. 1–53, doi:10.1130/SPE233-p1.
Gans, P.B., and Miller, E.L., 1983, Style of mid-Tertiary extension in east-central Nevada: Special Studies of the Utah Geological and Mineral Survey, v. 59, p. 107–160.
Gans, P.B., Repetski, J.E., Harris, A.G., and Clark, D.H., 1990, Conodont geothermometry of Paleozoic supracrustal rocks in the Eastern Great Basin, *in* Geological Society of Nevada Symposium, p. 103.
Garside, L.J., Henry, C.D., Faulds, J.E., and Hinz, N.H., 2005, The upper reaches of the Sierra Nevada auriferous gold channels, California and Nevada: Geological Society of Nevada Symposium, p. 209–235.
Gehrels, G.E., Valencia, V.A., and Pullen, A., 2006, Detrital Zircon Geochronology By Laser-Ablation Multicollector ICPMS At the Arizona Laserchron Center: Geochronology: Emerging Opportunities, v. 12, p. 67–76.
Gehrels, G.E., Valencia, V.A., and Ruiz, J., 2008, Enhanced precision, accuracy, efficiency, and spatial resolution of U-Pb ages by laser ablation-multicollector-inductively coupled plasma-

mass spectrometry: Geochemistry, Geophysics, Geosystems, v. 9, p. Q03017, doi:10.1029/2007GC001805.
Goldstrand, P.M., 1992, Evolution of Late Cretaceous and Early Tertiary Basins of Southwest Utah Based on Clastic Petrology: Journal of Sedimentary Research, v. Vol. 62, p. 495–507, doi:10.1306/D4267933-2B26-11D7-8648000102C1865D.
Goldstrand, P.M., 1994, Tectonic development of Upper Cretaceous to Eocene strata of southwestern Utah: Bulletin of the Geological Society of America, v. 106, p. 145–154, doi:10.1130/0016-7606(1994)106<0145.
Gooley, J.T., Grove, M.J., and Graham, S.A. TECTONIC EVOLUTION OF THE CENTRAL CALIFORNIA MARGIN AS REFLECTED BY DETRITAL ZIRCON COMPOSITION IN THE MOUNT DIABLO REGION: Geological Society of America Special Paper,.
Haynes, S.R., 2003, Development of the Eocene Elko Basin, northeastern Nevada: Implications for paleogeography and regional tectonism: The University of British Columbia, https://circle.ubc.ca/bitstream/id/34598/ubc_2003-0240.pdf.
Henry, C.D., 2008, Ash-flow tuffs and paleovalleys in northeastern Nevada: Implications for Eocene paleogeography and extension in the Sevier hinterland, northern Great Basin: Geosphere, v. 4, p. 1–35, doi:10.1130/GES00122.1.
Henry, C.D., 2018, The Eocene Elko Basin and Elko Formation, NE Nevada: Paleotopographic Controls on Area, Thickness, Facies Distribution, and Petroleum Potential: AAPG Annual Convention, v. May 20-23, p. 2857031.
Henry, C.D., Hinz, N.H., Faulds, J.E., Colgan, J.P., John, D.A., Brooks, E.R., Cassel, E.J., Garside, L.J., Davis, D.A., and Castor, S.B., 2012, Eocene-Early Miocene paleotopography of the Sierra Nevada-Great Basin-Nevadaplano based on widespread ash-flow tuffs and paleovalleys: Geosphere, v. 8, p. 1–27, doi:10.1130/GES00727.1.
Henry, C.D., Jackson, M.R., Mathewson, D.C., Koehler, S.R., and Moore, S.C., 2015, Eocene Igneous Geology and Relation to Mineralization: Railroad District, Southern Carlin Trend, Nevada, *in* Pennell, W.M. and Garside, L.J. eds., Geological Society of Nevada, New Concepts and Discoveries, p. 939–965.
Henry, C.D., and John, D.A., 2013, Magmatism, ash-flow tuffs, and calderas of the ignimbrite flareup in the western Nevada volcanic field, Great Basin, USA: Geosphere, v. 9, p. 951, doi:10.1130/GES00867.1.
Henry, C.D., McGrew, A.J., Colgan, J.P., Snoke, A.W., and Brueseke, M.E., 2011, Timing, distribution, amount, and style of Cenozoic extension in the northern Great Basin (J. P. Evans & J. Lee, Eds.): GSA Field Guide, v. 21, p. 27–66, doi:10.1130/2011.0021(02).
Horton, T.W., and Chamberlain, C.P., 2006, Stable isotopic evidence for Neogene surface downdrop in the central Basin and Range Province: Bulletin of the Geological Society of America, v. 118, p. 475–490, doi:10.1130/B25808.
Horton, T.W., Sjostrom, D.J., Abruzzese, M.J., Poage, M.A., Waldbauer, J.R., Hren, M.T., Wooden, J.L.P., and Chamberlain, C.P., 2004, Spatial and temporal variation of Cenozoic surface elevation in the Great Basin and Sierra Nevada: American Journal of Science, v. 304, p. 862–888, doi:10.2475/ajs.304.10.862.
Howard, K.A., Wooden, J.L., Barnes, C.G., Premo, W.R., Snoke, A.W., and Lee, S., 2011, Episodic growth of a Late Cretaceous and Paleogene intrusive complex of pegmatitic leucogranite, Ruby Mountains core complex, Nevada, USA: Geosphere, v. 7, p. 1220, doi:10.1130/GES00668.1.
Humphreys, E.D., 1995, Post-Laramide removal of the Farallon slab, western United States:

Geology, v. 23, p. 987, doi:10.1130/0091-7613(1995)023<0987:PLROTF>2.3.CO;2.
Kent-Corson, M.L., Sherman, L.S., Mulch, A., and Chamberlain, C.P., 2006, Cenozoic topographic and climatic response to changing tectonic boundary conditions in Western North America: Earth and Planetary Science Letters, v. 252, p. 453–466, doi:10.1016/j.epsl.2006.09.049.
Konstantinou, A., and Miller, E.L., 2015, Evidence for a long-lived accommodation/transfer zone beneath the Snake River Plain: A possible influence on Neogene magmatism? Tectonics, v. 34, p. 2387–2398, doi:10.1002/2015TC003863.
Konstantinou, A., Strickland, A., Miller, E.L., Fisher, C.M., Wooden, J.L.P., Valley, J.W., and Vervoort, J.D., 2013a, Magmatically induced diapiric rise of the Albion-Raft River-Grouse Creek metamorphic core complex, northeastern Basin and Range: Tectonics,.
Konstantinou, A., Strickland, A., Miller, E.L., and Wooden, J.P., 2012, Multistage Cenozoic extension of the Albion–Raft River–Grouse Creek metamorphic core complex: Geochronologic and stratigraphic constraints: Geosphere, v. 8, p. 1429–1466, doi:10.1130/GES00778.1.
Konstantinou, A., Valley, J.W., Strickland, A., Miller, E.L., Fisher, C.M., Vervoort, J.D., and Wooden, J.L.P., 2013b, Geochemistry and geochronology of the Jim Sage volcanic suite, southern Idaho: Implications for Snake River Plain magmatism and its role in the history of Basin and Range extension: Geosphere, v. 9, p. 1681–1703, doi:10.1130/GES00948.1.
Kreemer, C., Blewitt, G., and Hammond, W.C., 2010, Evidence for an active shear zone in southern Nevada linking the Wasatch fault to the Eastern California shear zone: Geology, v. 38, p. 475–478, doi:10.1130/G30477.1.
Lachenbruch, A.H., and Morgan, P., 1990, Continental extension, magmatism and elevation; formal relations and rules of thumb: Tectonophysics, v. 174, p. 39–62.
Larimer, J.E., Yanites, B.J., Phillips, W., and Mittelstaedt, E., 2019, Late Miocene rejuvenation of central Idaho landscape evolution: A case for surface processes driven by plume-lithosphere interaction: Lithosphere, v. 11, p. 59–72, doi:10.1130/L746.1.
Lechler, A.R., and Niemi, N.A., 2011a, Controls on the spatial variability of modern meteoric δ 18O: Empirical constraints from the western U.S. and east Asia and implications for stable isotope studies: American Journal of Science, v. 311, p. 664–700, doi:10.2475/08.2011.02.
Lechler, A.R., and Niemi, N.A., 2011b, Sedimentologic and isotopic constraints on the Paleogene paleogeography and paleotopography of the southern Sierra Nevada, California: Geology, v. 39, p. 379–382, doi:10.1130/G31535.1.
Lee, J., Blackburn, T., and Johnston, S., 2017, Timing of mid-crustal ductile extension in the northern Snake Range metamorphic core complex, Nevada: Evidence from U/Pb zircon ages: Geosphere, v. 13, p. 439–459, doi:10.1130/GES01429.1.
Lerch, D.W., Miller, E.L., McWilliams, M.O., and Colgan, J.P., 2008, Tectonic and magmatic evolution of the northwestern Basin and Range and its transition to unextended volcanic plateaus: Black Rock Range, Nevada: Bulletin of the Geological Society of America, v. 120, p. 300–311, doi:10.1130/B26151.1.
Levander, A., and Miller, M.S., 2012, Evolutionary aspects of lithosphere discontinuity structure in the western U.S.: Geochemistry, Geophysics, Geosystems, v. 13, p. n/a-n/a, doi:10.1029/2012GC004056.
Lofgren, D.L., Honey, J.G., McKenna, M.C., Zondervan, R.L., and Smith, E.E., 2008, Paleocene primates from the Goler Formation of the Mojave Desert in California, *in* Wang, X. and Barnes, L.G. eds., Science Series 41: Geology and Vertebrate Paleontology of Western and

Southern North America, Natural History Museum of Los Angeles County, p. 11–28.
Long, S.P., 2018, Geometry and extension magnitude of the Basin and Range Province (39°N), Utah, Nevada, and California, USA: Constraints from a province-scale cross section: Geological Society of America Bulletin, doi:10.1130/B31974.
Long, S.P., 2012, Magnitudes and spatial patterns of erosional exhumation in the Sevier hinterland, eastern Nevada and western Utah, USA: Insights from a Paleogene paleogeologic map: Geosphere, v. 8, p. 881, doi:10.1130/GES00783.1.
Ludwig, K.R., 2008, User's manual for Isoplot 3.7: A geochronological toolkit for Microsoft Excel: Berkeley Geochronology Center Special Publication No. 4, v. 4, p. 77.
Lund, K., 2008, Geometry of the Neoproterozoic and Paleozoic rift margin of western Laurentia: Implications for mineral deposit settings: Geosphere, v. 4, p. 429, doi:10.1130/GES00121.1.
Lund, K., Beard, L.S., and Perry, W.J., 1993, Relation between extensional geometry of the northern Grant Range and oil occurrences in Railroad Valley, east-central Nevada: AAPG Bulletin, v. 77, p. 945–962.
Lund Snee, J.-E., 2013, Geology and geochronology of Cenozoic units in the Piñon Range and Huntington Valley, Nevada: Stanford University, http://purl.stanford.edu/hx388mg6634.
Lund Snee, J.-E., and Miller, E.L., 2020, Data for Elko Basin, Nevada, geochronology and stable isotope analyses, 2015-2019:, https://purl.stanford.edu/mt578jx4294.
Lund Snee, J.-E., and Miller, E.L., 2015, Preliminary geologic map of Cenozoic units of the central Robinson Mountain volcanic field and northwestern Huntington Valley: Nevada Bureau of Mines and Geology Open File, v. 15–2, p. 42, http://pubs.nbmg.unr.edu/product-p/of2015-02.htm.
Lund Snee, J.-E., Miller, E.L., Grove, M., Hourigan, J.K.J.K., and Konstantinou, A., 2016, Cenozoic paleogeographic evolution of the Elko Basin and surrounding region, northeast Nevada: Geosphere, v. 12, p. 464–500, doi:10.1130/GES01198.1.
MacGinitie, H.D., 1941, Contributions to Paleontology: Middle Eocene FLora from the Central Sierra Nevada: Washington, D. C., Carnegie Institution of Washington Publication 534.
McCrory, P.A., Blair, J.L., Waldhauser, F., and Oppenheimer, D.H., 2012, Juan de Fuca slab geometry and its relation to Wadati-Benioff zone seismicity: Journal of Geophysical Research: Solid Earth, v. 117, doi:10.1029/2012JB009407.
McGrew, A.J., Peters, M.T., and Wright, J.E., 2000, Thermobarometric constraints on the tectonothermal evolution of the East Humboldt range metamorphic core complex, Nevada: Bulletin of the Geological Society of America, v. 112, p. 45–60, doi:10.1130/0016-7606(2000)112<45:TCOTTE>2.0.CO;2.
McGrew, A.J., and Snee, L.W., 1994, 40Ar/39Ar thermochronologic constraints on the tectonothermal evolution of the Northern East Humboldt range metamorphic core complex, Nevada: Tectonophysics, v. 238, p. 425–450, doi:10.1016/0040-1951(94)90067-1.
McQuarrie, N., and Chase, C.G., 2000, Raising the Colorado Plateau: Geology, v. 28, p. 91, doi:10.1130/0091-7613(2000)028<0091:RTCP>2.0.CO;2.
McQuarrie, N., and Wernicke, B.P., 2005, An animated tectonic reconstruction of southwestern north america since 36 Ma: Geosphere, v. 1, p. 147–172, doi:10.1130/GES00016.1.
Miller, E.L., Dumitru, T.A., Brown, R.W., and Gans, P.B., 1999, Rapid Miocene slip on the Snake Range–Deep Creek Range fault system, east-central Nevada: Geological Society of America Bulletin, v. 111, p. 886–905, doi:10.1130/0016-7606(1999)111<0886:RMSOTS>2.3.CO;2.
Miller, E.L., and Gans, P.B., 1989, Cretaceous crustal structure and metamorphism in the

hinterland of the Sevier thrust belt, western U.S. Cordillera: Geology, v. 17, p. 59–62, doi:10.1130/0091-7613(1989)017<0059.
Miller, E.L., Konstantinou, A., and Strickland, A., 2012, Comment on "Geodynamics of synconvergent extension and tectonic mode switching: Constraints from the Sevier-Laramide orogen" by Michael L. Wells et al.: Tectonics, v. 31, p. n/a-n/a, doi:10.1029/2012TC003103.
Mix, H.T., Mulch, A., Kent-Corson, M.L., and Chamberlain, C.P., 2011, Cenozoic migration of topography in the North American Cordillera: Geology, v. 39, p. 87–90, doi:10.1130/G31450.1.
Mulch, A., Chamberlain, C.P., Cosca, M.A., Teyssier, C., Methner, K., Hren, M.T., and Graham, S.A., 2015, Rapid change in high-elevation precipitation patterns of western North America during the Middle Eocene Climatic Optimum (MECO): American Journal of Science, v. 315, p. 317–336, doi:10.2475/04.2015.02.
Noble, D.C., 1972, Some observations on the Cenozoic volcano-tectonic evolution of the Great Basin, western United States: Earth and Planetary Science Letters, v. 17, p. 142–150, doi:10.1016/0012-821X(72)90269-5.
Parsons, T., Thompson, G.A., and Sleep, N.H., 1994, Mantle plume influence on the Neogene uplift and extension of the US western Cordillera? Geology, v. 22, p. 83–86, doi:10.1130/0091-7613(1994)022<0083:MPIOTN>2.3.CO;2.
Pearson, P.N., Ditchfield, P.W., Singano, J., Harcourt-Brown, K.G., Nicholas, C.J., Olsson, R.K., Shackleton, N.J., and Hall, M.A., 2001, Warm tropical sea surface temperatures in the Late Cretaceous and Eocene epochs: Nature, v. 413, p. 481.
Pierce, K.L., and Morgan, L.A., 2009, Is the track of the Yellowstone hotspot driven by a deep mantle plume? --- Review of volcanism, faulting, and uplift in light of new data: Journal of Volcanology and Geothermal Research, v. 188, p. 1–25, doi:10.1016/j.jvolgeores.2009.07.009.
Pierce, K.L., Morgan, L.A., and Link, P.K., 1992, The track of the Yellowstone hot spot: Volcanism, faulting, and uplift: Regional geology of eastern Idaho and western Wyoming: Geological Society of America Memoir, v. 179, p. 1–53.
Poage, M.A., and Chamberlain, C.P., 2001, Empirical relationships between elevation and the stable isotope composition of precipitation and surface waters: Considerations for studies of paleoelevation change: American Journal of Science, v. 301, p. 1–15, doi:10.2475/ajs.301.1.1.
Poage, M.A., and Chamberlain, C.P., 2002, Stable isotopic evidence for a Pre-Middle Miocene rain shadow in the western Basin and Range: Implications for the paleotopography of the Sierra Nevada: Tectonics, v. 21, p. 16-1-16–10, doi:10.1029/2001TC001303.
Regnier, J., 1960, Cenozoic geology in the vicinity of Carlin, Nevada: Bulletin of the Geological Society of America, v. 71, p. 1189–1210, doi:10.1130/0016-7606(1960)71[1189:CGITVO]2.0.CO;2.
Ressel, M.W., and Henry, C.D., 2006, Igneous geology of the Carlin trend, Nevada: Development of the Eocene plutonic complex and significance for Carlin-type gold deposits: Economic Geology, v. 101, p. 347–383, doi:10.2113/gsecongeo.101.2.347.
Ruksznis, A., 2015, Geology and geochronology of Cenozoic sedimentary basins, east-central Nevada: Stanford University, 219 p.
Ryskamp, E.B., Abbott, J.T., Christiansen, E.H., Keith, J.D., Vervoort, J.D., and Tingey, D.G., 2008, Age and petrogenesis of volcanic and intrusive rocks in the Sulphur Spring Range,

central Nevada: Comparisons with ore-associated Eocene magma systems in the Great Basin: Geosphere, v. 4, p. 496, doi:10.1130/GES00113.1.
Saleeby, J.B., Ducea, M.N., Busby, C.J., Nadin, E.S., and Wetmore, P.H., 2008, Chronology of pluton emplacement and regional deformation in the southern Sierra Nevada batholith, California: Special Paper of the Geological Society of America, v. 438, p. 397–427, doi:10.1130/2008.2438(14).
Sharman, G.R., Graham, S.A., Grove, M., Kimbrough, D.L., and Wright, J.E., 2015, Detrital zircon provenance of the late Cretaceous-Eocene California forearc: Infl uence of laramide low-angle subduction on sediment dispersal and paleogeography: Bulletin of the Geological Society of America, v. 127, p. 38–60, doi:10.1130/B31065.1.
Sharp, R.P., 1939, The Miocene Humboldt Formation in Northeastern Nevada: The Journal of Geology, v. 47, p. 133–160, doi:10.1086/624749.
Shen, W., and Ritzwoller, M.H., 2016, Crustal and uppermost mantle structure beneath the United States: Journal of Geophysical Research: Solid Earth, v. 121, p. 4306–4342, doi:10.1002/2016JB012887.
Smith, M.E., Cassel, E.J., Jicha, B.R., Singer, B.S., and Canada, A.S., 2017, Hinterland drainage closure and lake formation in response to middle Eocene Farallon slab removal, Nevada, U.S.A.: Earth and Planetary Science Letters, v. 479, p. 156–169, doi:10.1016/j.epsl.2017.09.023.
Smith, J.F.J., and Howard, K.A., 1977, Geologic map of the Lee Quadrangle (1:62,500 scale): US Geological Survey Map GQ-1393,.
Smith, J.F.J., and Ketner, K.B., 1978, Geologic map of the Carlin-Pinon Range area, Elko and Eureka counties, Nevada: U.S. Geological Survey Miscellaneous Investigations Series I-1028,.
Smith, J.F.J., Ketner, K.B., and Mabey, D.R., 1976, Stratigraphy of post-Paleozoic rocks and summary of resources in the Carlin-Pinon Range area, Nevada: United States Geological Survey Professional Paper, v. 867-B, p. 1–48.
Smith, D.L., Miller, E.L., Wyld, S.J., and Wright, J.E., 1993, Progression and timing of Mesozoic crustal shortening in the northern Great Basin, Western U.S.A, *in* Mesozoic Paleogeography of the Western United States-II, v. 71, p. 389–406, http://archives.datapages.com.stanford.idm.oclc.org/data/pac_sepm/088/088001/pdfs/389.pdf.
Snell, K.E., Koch, P.L., Druschke, P., Foreman, B.Z., and Eiler, J.M., 2014, High elevation of the 'Nevadaplano' during the Late Cretaceous: Earth and Planetary Science Letters, v. 386, p. 52–63, doi:10.1016/j.epsl.2013.10.046.
Sonder, L.J., England, P.C., Wernicke, B.P., and Christiansen, R.L., 1987, A physical model for Cenozoic extension of western North America: Geological Society, London, Special Publications, v. 28, p. 187–201, doi:10.1144/GSL.SP.1987.028.01.14.
Spencer, J.E., and Normark, W.R., 1979, Tosco-Abreojos fault zone: A Neogene transform plate boundary within the Pacific margin of southern Baja California, Mexico: Geology, v. 7, p. 554–557, doi:10.1130/0091-7613(1979)7<554:TFZANT>2.0.CO;2.
Stewart, J.H., 1980, Geology of Nevada: Nevada Bureau of Mines and Geology, Special Publication, v. 4, p. 136.
Stock, J.M., and Hodges, K. V., 1989, Pre-Pliocene Extension around the Gulf of California and the transfer of Baja California to the Pacific Plate: Tectonics, v. 8, p. 99–115, doi:10.1029/TC008i001p00099.

Stockli, D.F., 2005, Application of Low-Temperature Thermochronometry to Extensional Tectonic Settings: Reviews in Mineralogy and Geochemistry, v. 58, p. 411–448, doi:10.2138/rmg.2005.58.16.

Stockli, D.F., Surpless, B., Dumitru, T.A., and Farley, K. a., 2002, Thermochronological constraints on the timing and magnitude of Miocene and Pliocene extension in the central Wassuk Range, western Nevada: Tectonics, v. 21, p. 10–19, doi:10.1029/2001TC001295.

Strickland, A., Miller, E.L., Wooden, J.L., Kozdon, R., and Valley, J.W., 2011, Syn-extensional plutonism and peak metamorphism in the albion-raft river-grouse creek metamorphic core complex: American Journal of Science, v. 311, p. 261–314, doi:10.2475/04.2011.01.

Surpless, B., Stockli, D.F., Dumitru, T.A., and Miller, E.L., 2002, Two-phase westward encroachment of Basin and range extension into the northern Sierra Nevada: Tectonics, v. 21, p. 2-1-2–13, doi:10.1029/2000TC001257.

Taylor, W.J., Bartley, J.M., Martin, M.W., Geissman, J.W., Walker, J.D., Armstrong, P.A., and Fryxell, J.E., 2000, Relations between hinterland and foreland shortening: Sevier orogeny central North American Cordillera: Tectonics, v. 19, p. 1124–1143, doi:10.1029/1999TC001141.

Thatcher, W., Foulger, G.R., Julian, B.R., Svarc, J., Quilty, E., and Bawden, G.W., 1999, Present-Day Deformation Across the Basin and Range Province, Western United States: Science, v. 283, p. 1714–1717, doi:10.1126/science.283.5408.1714.

Tian, Y., and Zhao, D., 2012, P-wave tomography of the western United States: Insight into the Yellowstone hotspot and the Juan de Fuca slab: Physics of the Earth and Planetary Interiors, v. 200–201, p. 72–84, doi:10.1016/j.pepi.2012.04.004.

Tosdal, R.M., Wooden, J.L., Kistler, R.W., and Cluer, J.K., 2000, Geometry of the Neoproterozoic continental break-up, and implications for location of Nevadan mineral belts: Geology and ore deposits, p. 451–466.

Wallace, A.R., Perkins, M.E., and Fleck, R.J., 2008, Late Cenozoic paleogeographic evolution of northeastern Nevada: Evidence from the sedimentary basins: Geosphere, v. 4, p. 36–74, doi:10.1130/GES00114.1.

Wells, M.L., and Hoisch, T.D., 2012, Reply to comment by E. L. Miller et al. on “Geodynamics of synconvergent extension and tectonic mode switching: Constraints from the Sevier-Laramide orogen”: Tectonics, v. 31, p. n/a-n/a, doi:10.1029/2012TC003136.

Wells, M.L., Hoisch, T.D., Cruz-Uribe, A.M., and Vervoort, J.D., 2012, Geodynamics of synconvergent extension and tectonic mode switching: Constraints from the Sevier-Laramide orogen: Tectonics, v. 31, p. 1–20, doi:10.1029/2011TC002913.

Wolfe, J.A., Forest, C.E., and Molnar, P., 1998, Paleobotanical evidence of Eocene and Oligocene paleoaltitudes in midlatitude western North America: Bulletin of the Geological Society of America, v. 110, p. 664–678, doi:10.1130/0016-7606(1998)110<0664:PEOEAO>2.3.CO;2.

Wolfe, J.A., Schorn, H.E., Forest, C.E., and Molnar, P., 1997, Paleobotanical evidence for high altitudes in Nevada during the Miocene: Science, v. 276, p. 1672–1675, doi:10.1126/science.276.5319.1672.

Yeend, W.R., 1974, Gold-Bearing Gravels of the Ancestral Yuba River, Sierra Nevada, California: USGS Professional Paper, v. 772.

Zachos, J., Pagani, M., Sloan, L., Thomas, E., and Billups, K., 2001, Trends, Rythms, and Aberration in Global Climate 65 Ma to Present: Science, v. 292, p. 686–693, doi:10.1126/science.1059412.